



HAL
open science

Modeling of continental weathering under high-CO₂ atmospheres during Precambrian times

Sébastien Fabre, Gilles Berger, Anne Nédélec

► **To cite this version:**

Sébastien Fabre, Gilles Berger, Anne Nédélec. Modeling of continental weathering under high-CO₂ atmospheres during Precambrian times. *Geochemistry, Geophysics, Geosystems*, 2011, 12, pp.10,001. 10.1029/2010GC003444 . insu-03620191

HAL Id: insu-03620191

<https://insu.hal.science/insu-03620191>

Submitted on 25 Mar 2022

HAL is a multi-disciplinary open access archive for the deposit and dissemination of scientific research documents, whether they are published or not. The documents may come from teaching and research institutions in France or abroad, or from public or private research centers.

L'archive ouverte pluridisciplinaire **HAL**, est destinée au dépôt et à la diffusion de documents scientifiques de niveau recherche, publiés ou non, émanant des établissements d'enseignement et de recherche français ou étrangers, des laboratoires publics ou privés.

Copyright



Modeling of continental weathering under high-CO₂ atmospheres during Precambrian times

Sébastien Fabre

*Université de Toulouse, UPS-OMP, GET, 14 avenue Edouard Belin, F-31400 Toulouse, France
(fabre@lmtg.obs-mip.fr)*

CNRS, IRAP, 14 avenue Edouard Belin, F-31400 Toulouse, France

Gilles Berger

Observatoire Midi-Pyrénées, IRAP, UMR 5277, 14 avenue Edouard Belin, F-31400 Toulouse, France

Anne Nédélec

Université de Toulouse, UPS-OMP, GET, 14 avenue Edouard Belin, F-31400 Toulouse, France

[1] Batch experiments were conducted to simulate abiotic weathering of the continental crust under high-CO₂ atmospheric conditions during Precambrian times, i.e., corresponding to the general Archaean conditions as well as to the immediate aftermath of the Neoproterozoic Snowball Earth ice ages. Three types of rock (basalt, granodiorite and tonalite) representative of the Archaean to Proterozoic continental crust were reacted in the form of powders for 1 year at 40°C with pure water under various water/rock ratios, in oxic and anoxic atmospheres containing 10% CO₂, that is, under conditions assumed to characterize the greenhouse effect which prevailed at that time. Chemical and mineralogical data collected during the course of the experiments reflect alteration phenomena occurring in two steps: (1) rapid leaching of the fresh surfaces, probably related to the proton-donor capacity of the CO₂ and (2) a steady state reaction under near-neutral conditions. These observed dissolution rates can be satisfactorily modeled by kinetic data available in the literature. Using a 1-D weathering model reproducing the two steps, we evaluate the atmospheric CO₂ consumption rate at the Snowball Earth aftermath, focusing on the relative contribution of surface leaching versus steady state reaction. The results show that the process is dominated by surface exchange.

Components: 12,200 words, 10 figures, 9 tables.

Keywords: Precambrian; atmospheric CO₂; chemical weathering; experiments.

Index Terms: 1039 Geochemistry: Alteration and weathering processes (3617).

Received 22 November 2010; **Revised** 28 July 2011; **Accepted** 4 August 2011; **Published** 4 October 2011.

Fabre, S., G. Berger, and A. Nédélec (2011), Modeling of continental weathering under high-CO₂ atmospheres during Precambrian times, *Geochem. Geophys. Geosyst.*, 12, Q10001, doi:10.1029/2010GC003444.

1. Introduction

[2] It is now broadly accepted that weathering-aggressive climatic conditions strongly affected Archaean sedimentary deposits and source rocks.

Field evidence for aggressive chemical weathering in the past includes the washing out from sedimentary formations of clay minerals such as kaolinite, primarily produced from the chemical alteration of feldspars, together with smectites derived from the

erosion of abundant volcanic rocks, leaving the more stable minerals, such as quartz, to dominate the framework mineralogy [Eriksson *et al.*, 2004]. The introduction of the CIA (Chemical Index of Alteration) by Nesbitt and Young [1982], used as an indicator of palaeoweathering, applied to shales of late Archaean to Neoproterozoic age, generally supports the hypothesis of increased chemical weathering during the Archaean [Condie, 2001].

[3] Several atmospheric controlling factors for continental weathering can be inferred for the early Precambrian: increased temperatures [Kasting, 1993], humidity [Des Marais, 1994] and concentrations of greenhouse gases such as methane [Pavlov *et al.*, 2001; Kasting and Siefert, 2002] and carbon dioxide [Young, 1991; Kasting, 1993]. In this latter case, CO₂ gas dissolved in rainwater yields a weak acid that can lead to the chemical attack of rocks. Clearly, the weathering intensity will depend on the CO₂ partial pressure (pCO₂) in the atmosphere.

[4] Since the work of Walker *et al.* [1981], it has been established that, on the geological time scale, the carbon-cycle is mainly driven by two processes: (1) CO₂ degassing related to active margin and mid-ocean ridge volcanic activity, as well as metamorphism of carbonate rocks [Kerrick, 2001] and (2) CO₂ consumption through weathering of continental silicate rocks and storage of organic carbon in sediments. The overall reaction for chemical weathering of Ca-silicates can be written as: CaSiO₃ + CO₂ = CaCO₃ + SiO₂ [Berner and Berner, 1987].

[5] The carbonate-silicate weathering cycle may act as a stabilizing influence on the Earth's climate through a negative feedback [Walker, 1990]. Several periods of Earth history, especially the Archaean, are characterized by evidence of very high CO₂ partial pressures. Minerals acting as CO₂-barometers and other features of the Archaean sedimentary record indicate that there were higher levels of CO₂ in the Archaean atmosphere than today. In some cases, these indicators allow a quantification of CO₂ levels. For instance, Rye *et al.* [1995] used carbonate-silicate equilibrium in the 2.75-Ga Mount Roe palaeosol to estimate the partitioning of CO₂ between soil and air in the late Archaean. Their calculations suggest a maximum CO₂ partial pressure of 10^{-1.4} atm (ca. 100 times Present Atmospheric Level = PAL = 0.04 atm), significantly lower than the estimate of Lowe and Tice [2004] - between 1.4 and 10 (50–300 PAL) - based on the existence of nahcolite (NaHCO₃) % in Pilbara sediments.

[6] Whatever the case, we can suppose that, during Archaean times, the weathering intensity and,

consequently, the CO₂ consumption, was higher than at the present-day, although likely balanced by higher CO₂ inputs. To quantify the CO₂ consumption linked to mineral dissolution in Precambrian times, we may consider two main types of approaches. On one hand, field studies can lead to a parametric approach in which climatic parameters (mean annual temperature and runoff) are linked to CO₂ consumption by the dissolution of silicate minerals [Brady, 1991, White and Blum, 1995; Dessert *et al.*, 2001, Oliva *et al.*, 2003]. However, such studies often validate only a limited data set, in this case modern environmental conditions (see particularly Oliva *et al.* [2003]), so any extrapolation toward past conditions is speculative. On the other hand, an alternative approach has been developed based on physico-chemical transfer between the atmosphere-hydrosphere and the continental crust. For example, Higgins and Schrag [2003] used a three-box model for the ocean-atmosphere system. In this model, a super-greenhouse effect drives a hyper-active hydrological cycle inducing intense continental weathering, such that CO₂ levels could be drawn down from very high levels to pre-glacial levels in about 200 kyr. By contrast, Le Hir *et al.* [2009] used a combination of Global Climate Modeling (FOAM) and weathering simulation programs to propose a much longer time interval, ca 3 Myr, for erasing these post-glacial perturbations. The main criticism of such studies is that they are calibrated on present-day conditions.

[7] This study is focused on the microscopic scale, by combining appropriate experiments on water-gas interactions with numerical formalism, taking into account the phenomenology of reactions at the solid-solution interface. In detail, the present study aims to characterize continental silicate weathering under a warm and CO₂-rich atmosphere. Laboratory experiments were carried out over a duration of 1 year to evaluate the silicate weathering rate and the CO₂ consumption as a function of the presence or absence of oxygen (hence the influence of ferric or ferrous iron on the alteration sequence) and the impact of the surface area exposed to alteration. The experimental results are used to calibrate standard numerical model simulations against the long-term experimental observations, since short-term theoretical kinetic constants measured in the laboratory are well known to produce overestimated values when compared to field data [Brantley, 2003; White and Brantley, 2003]. This first part of the paper describes the experiments conducted in the glove-box and the principle of the numerical model. Then, the model is extrapolated

Table 1. Percentage (Surface) of Various Minerals in the Three Rocks Determined by Image and Modal Analysis

Flood Basalt	%	Granodiorite	%	Tonalite	%
<i>Percentage (Surface) of Various Minerals in the Three Rocks Calculated for the Numerical Modeling</i>					
Albite	23	Quartz	25	Quartz	25
Anorthite	22	Albite	25	Albite	27.8
Diopside	19	Anorthite	19	Anorthite	10.76
Hedenbergite	18	K-feldspar	13	Orthose	1.19
Ilmenite	6	Phlogopite	4	Phlogopite	8.5
Crypto-cristalline matrix	12	Annite	8	Annite	6.5
		Amphibole	6	Amphibole	5
				Diospide	9
				Hedenbergite	6
sum.	100		100		99.75
<i>Percentage (Surface) of Various Minerals Determined by Image Analysis</i>					
Plagioclase	45	Quartz	25	Quartz	25
Clinopyroxene	37	Plagioclase	44	Plagioclase	39.0
Oxides	6	K-feldspar	13	K-feldspar (?)	
Crypto-cristalline matrix	12	Biotite	12	Biotite	16
		Green horblende	6	Amphibole	5
				Clinopyroxene	15
sum.	100		100		100
<i>Major Elements Composition (wt.%)</i>					
SiO ₂	49.2		65.6		67.5
TiO ₂	3.49		0.57		
Al ₂ O ₃	12.98		15.9		15.97
Fe ₂ O ₃ *	14.53		5		3.7
MnO	0.18		0.08		0.06
MgO	5.17		1.65		1.64
CaO	9.14		3.75		3.96
Na ₂ O	2.17		3		4.67
K ₂ O	1.00		3.75		1.87
H ₂ O	1.99		0.15		0
P ₂ O ₅	0.41				0.17
sum.	100.28		98.95		99.51

to the geological time-scale and past conditions, leading us to evaluate the CO₂ consumption rate with respect to physical factors such as soil texture and drainage intensity (see section 5).

2. Nature and Origin of Samples

[8] Four kinds of rock sample were used for this study, namely, tonalite, granodiorite and two different types of basalt. These rock samples are thought to be representative of the Archaean continental crust. The selected samples are relatively well preserved from alteration. When present, the secondary phases are described in the following petrographic section.

2.1. Tonalite

[9] The selected tonalite is a member of the 2.9-Ga-old so-called TTG suite (Tonalites-Trondhjemites-Granodiorites) from the Archaean Ntem Complex of South Cameroon [Nédélec et al., 1990; Shang et al., 2004]. TTGs are regarded as constituents of proto-

continents worldwide [Martin, 1994; Martin and Moyen, 2002, and references therein]. Hence, they are an ideal material to study Archaean continental weathering. The present specimen (AN 84) is heterogranular, with abundant plagioclase (An 27) and quartz. Ferromagnesian phases are represented by slightly altered diopside ($X_{Mg} \approx 0.76$), hornblende and high-Ti biotite ($X_{Mg} \approx 0.58$, $Ti \approx 0.6$ apfu – atom per formula unit), while the accessories are made up of opaque minerals (magnetite and ilmenite) as well as apatite and zircon. The secondary minerals are chlorite, epidote and scarce calcite. The whole-rock composition (Table 1) is relatively silicic (silica content: 67.47 wt %) and sodic ($K_2O/Na_2O \approx 0.4$), as expected for a typical Archaean TTG [Martin, 1994].

2.2. Granodiorite

[10] A granodiorite was also selected, because the modern continental crust is mainly composed of granites and granodiorites, with an approximately mafic granodioritic composition [Wedepohl, 1995].

Table 2. Physical Characteristic of the Rock Powders

	Basalt		Granodiorite		Tonalite	
	80–125	125–500	80–125	125–500	80–125	125–500
Grain-size (mm)	80–125	125–500	80–125	125–500	80–125	125–500
Surface (m ² /g) (BET)	1.7	1.19	0.495	0.2	0.493	0.169
W/R: water mass/rock mass	3.3	70	3.3	70	3.3	70

The sample comes from the high-K Mont-Louis Andorra Variscan pluton (eastern Pyrenees, France), which has an outcrop area of 600 km². The rock is medium- to coarse-grained (5–10 mm) and moderately isogranular. Major minerals are subautomorphic zoned plagioclase (An 51 to An 29) with frequently altered calcic cores, quartz and interstitial slightly perthitic orthoclase. Mafic silicates are biotite and subordinate hornblende. Accessory minerals are ilmenite, apatite and zircon. The whole-rock composition (n°37 in the study by Gleizes *et al.* [1993]) is presented in Table 1. It is noteworthy that this granodiorite is slightly less silicic (65.6 wt%) and more potassic (K₂O/Na₂O ≈ 1.25) than the Achaean tonalite sample, and is therefore representative of the evolution of the continental crust through geological time.

2.3. Tholeiitic Flood Basalt

[11] A basalt sample was collected from the Paraná large igneous province of southern Brazil [Harry and Sawyer, 1992; Hawkesworth *et al.*, 1992, 2000; Kirstein *et al.*, 2001]. These flood basalts extend over an area of 1.5 × 10⁶ km² and may contain up to 2.35 × 10⁶ km³ of extrusive volcanics [Gladczenko *et al.*, 1997]. Eruptions in the Paraná Province began 133 (±1) Ma ago [Renne *et al.*, 1992], and ⁴⁰Ar-³⁹Ar ages from the whole area indicate that the entire province would have formed in an interval of 0.6 (±1) Ma [Renne *et al.*, 1996]. The selected sample, a Pitanga-type basalt (i.e. high Ti/Y), was collected near Uberaba (Minas Gerais, Brazil) and obtained by courtesy of Dr Leila Marques (IAG, Univ. Sao Paulo). The rock contains rare phenocrysts (pyroxenes) and numerous microlites of zoned plagioclase (An 64–36, with an average labradorite composition An 56), clinopyroxene (augite with X_{Mg} ≈ 0.74), and opaque minerals in a cryptocrystalline (devitrified) matrix of the same composition. Rounded vesicles are the most striking feature, and rare phyllosilicates provide evidence of minor post-magmatic fluid-rock interactions [Schenato, 1997; Scopel, 1997]. The rock has a typical tholeiitic composition (Table 1).

2.4. Island Arc Tholeiitic Basalt

[12] This second tholeiitic sample was only used in the first series of experiments. It originates from the

southern part of the island of Sulawesi (Indonesia). This rock comes from a thick flow unit belonging to the Bua formation of Eocene age [Polvé *et al.*, 1997], and is thus fully crystallized with abundant large zoned phenocrysts of diopside (X_{Mg} ≈ 0.95–0.77) and subordinate olivine (X_{Mg} ≈ 0.73–0.57) locally altered to iddingsite. It contains abundant microcrysts of clinopyroxene and plagioclase (An 86–72). Table 1 reports the major element composition, which is typical of high-alumina basalts of such subduction-related settings.

3. Methods

3.1 Sample Preparation

[13] Rocks were mechanically crushed, sieved into size fractions and cleaned with ultrapure water in an ultrasonic bath to remove the tiny highly reactive particles. Two fractions were prepared: 80–125 μm and 125–500 μm, respectively referred to as “fine” and “coarse.” The surface area of each fraction was measured by the B.E.T. method (Autosorb, Quantachrome) using Kr and N₂ as adsorbant gases; the measured values are reported in Table 2.

[14] Image analysis of thin sections and calculations based on the bulk chemistry published in the previously cited studies allowed us to assess the modal percentage of the various minerals forming the three rocks (Table 1). In detail, the BET-measured surface of each of the rock powders was attributed to the different mineral species according to their normative percentages. This assumes that the different minerals have the same crushing behavior, which is likely not true. However, among the expected reactive minerals, plagioclases and pyroxenes are the most abundant and probably have nearly similar crushing behavior (when compared to phyllosilicates). We should point out that grains were observed to be polymineralic (data not shown).

3.2. Experimental Protocol

[15] A first set of duplicate experiments was conducted for 12 months, (1) under oxidizing conditions in a 10% CO₂ – 90% air mixture, and (2) under anoxic conditions in a 10% CO₂ – 90% N₂ mixture. At intervals of 3, 6 and 12 months, a container was

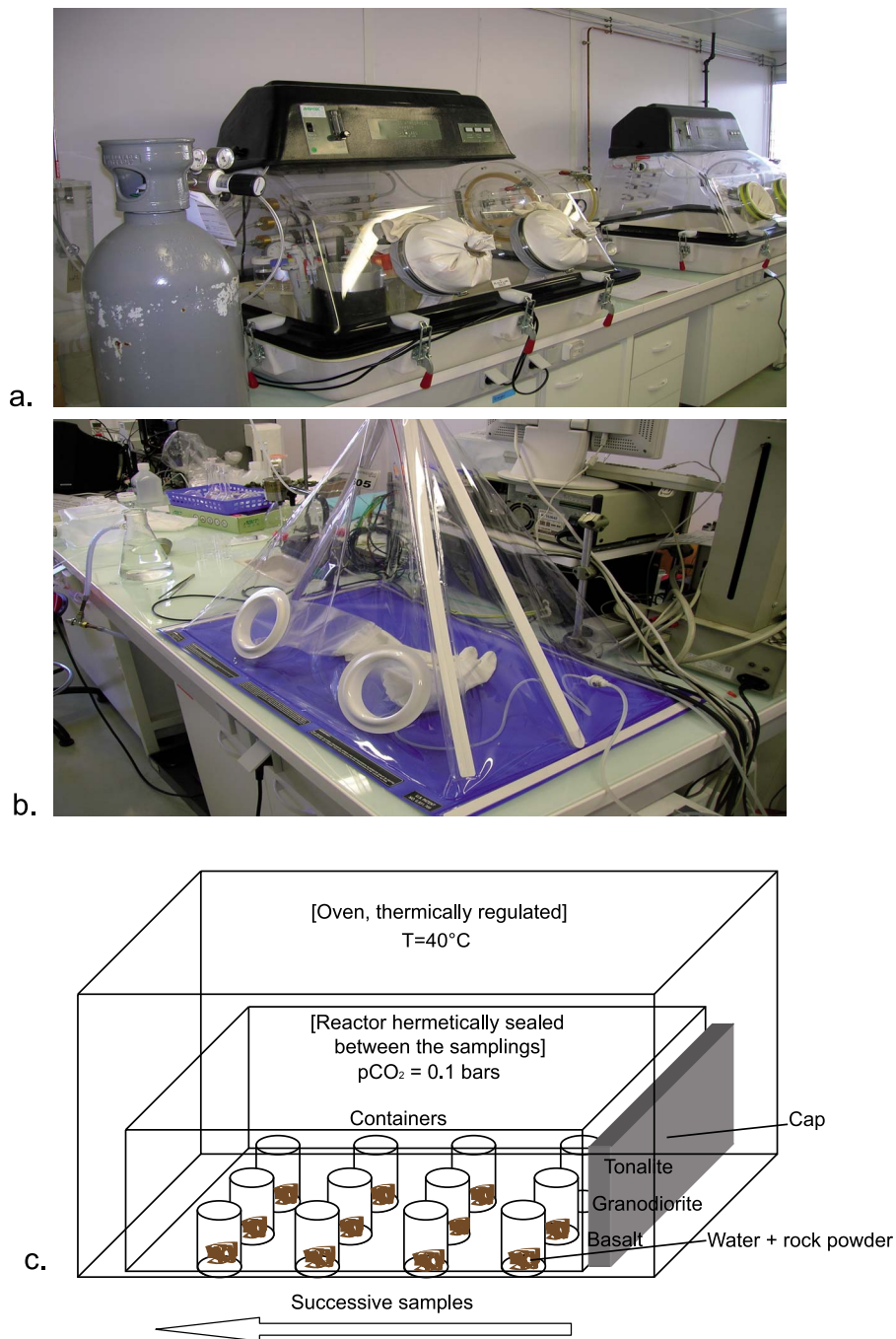


Figure 1. (a) View of the static glove-box in which rock powder, water and measurement devices were degassed. (b) View of the disposable globe-box filled with a gas mix of N₂ (90%) – CO₂ (10%), in which samplings and measurements were done each month. (c) Sketch of the experimental device, namely the reactor enclosed in the oven. The reactor was organized as follows: from right to left, successive polypropylene containers (one for each sampling time) used for sampling and in situ pH-Eh measurements and from back to front, the three types of rocks.

removed from each reactor for fluid monitoring and analysis of solids.

[16] For each experiment, 1 mg of fine rock powder and 4 mg of coarse rock powder, along with 1.5 and 5 mL of pure water (18 MΩ) respectively, were

introduced into six 30-mL open polypropylene containers (one per time interval and one per rock type), which were then placed inside a glass bottle filled with the gas mixture (Figure 1c). The glass bottles, here termed the “reactors,” were hermetically sealed and maintained for several months at

40°C in an oven, except for periods of a few minutes at room temperature during which the containers were removed for sampling. In each reactor, another container with pure water was added as a reference to monitor the potential pCO₂ variations by measuring pH during the course of the experiment. The nominal pH value for water equilibrated with pCO₂ = 0.1 bars is 4.5.

[17] The filling of the reactors with gas, the introduction or removal of the 30-mL polypropylene containers into or from the reactor, the estimation of pCO₂ by pH measurement and all the manipulations of the reacted samples were carried out in a glove box (Figures 1a and 1b) containing 10% CO₂, under either oxic or anoxic conditions depending on the experimental series. Under anoxic conditions, the low level of O₂ concentration is obtained by a Pd catalyst and measured by a dedicated sensor (for details, see *Mansour et al.* [2010]). In addition, Eh (reported in Appendix B) was monitored together with pH at each sampling. The sampling of solution-rock assemblages at regular time intervals provided the opportunity to renew the reactor atmosphere to compensate for the CO₂ consumption by rock sample alteration.

[18] An additional series of experiments was conducted to assess weathering rates far from chemical equilibrium and under constant pCO₂, using the coarse rock fraction (125–500 μm), and applying the same protocol except for the rock/solution/gas ratio (100 mg of rock sample and 7 mL of water by run, and a large 30-L polypropylene bottle as reactor filled with a CO₂-N₂ gas mixture). The experimental run duration was 5 months in this case (Figure 1c). Experimental conditions (grain-size, water/rock ratio and surface area) are listed in Table 2.

3.3. Solution Analyses

[19] Eh and pH were measured directly in the solution at room temperature in a disposable glove box (Figure 1b) corresponding to the experimental atmosphere using a WRW IS 160 pH-meter coupled to an Orion electrode. The pH of the pure solution used to monitor the CO₂ content in the reactor atmosphere remained close to a value of 4.55, which corresponds to the theoretical equilibrium of pure water at 0.1 bar CO₂.

[20] The aluminum and iron concentrations of the solutions were determined by inductively coupled plasma mass spectrometry (ICP-MS, Perkin-Elmer Elan 5000), and flame spectroscopy (Perkin Elmer Zeeman 5000) for K, Na, Mg and Ca after addition

of 2% HNO₃. Anion concentrations were measured by ion chromatography (Dionex ICS 2000). The aqueous silica concentration was measured using the molybdate method [*Strickland and Parsons*, 1972] with a Technicon analyzer II colorimeter. Given the small volume of experimental solution (a few mL), the bicarbonate concentration was not measured by conventional methods, but estimated as the charge difference between the measured cations and anions.

3.4. Secondary Phases

[21] At the end of each time interval, the altered samples were observed by scanning electronic microscopy (SEM, Jeol 6400). The accelerating voltage was 120 kV, and semiquantitative chemical analyses were performed at the local scale (spot size of about 25 nm) by X-ray fluorescence (EDS) using a point mode and without standards. The chemical spectra obtained were sufficient to confirm the mineral identification.

[22] The alteration phases were detached from the altered grains by ultrasonic treatment (VibraCell 75021, 100W). The fine particles were separated from the coarse grains by decanting, and were assumed to represent the entire secondary mineral fraction. This fine fraction was dried and weighed to a precision of 0.01 mg in order to determine the quantity of altered phases produced by the experimental weathering. However, some of the recovered fine particles may be derived from the original unaltered material. This fraction was evaluated at between 2.28 mg (granodiorite) and 0.51 mg (tonalite) by applying the same protocol to the unaltered samples, and was therefore subtracted from the raw data. The mineralogical composition of the altered samples was also determined by X-ray diffraction on oriented and glycolated preparations using Cu Kα radiation.

4. Results

4.1. Leaching Under Oxic and Anoxic Atmosphere at W/R = 1 and 5

[23] Table 3a presents the results of the first series of 1 year experiments. In Figure 2a, alkalinity and pH data under oxidizing conditions are plotted against their equivalent in anoxic experiments. For alkalinity, no significant difference can be observed between oxic and anoxic conditions: the intercept of the calculated correlation line is close to zero with a slope of ca. 1. In the case of pH, the values are

Table 3a (Sample). Experimental Results for the First Set of Experiments^a [The full Table 3a is available in the HTML version of this article]

	Sample		pH	Ca ²⁺	K ⁺	Na ⁺	Mg ²⁺	Fe ²⁺	Al ³⁺
<i>Time = 12 Months</i>									
Anoxic Atmosphere	Flood Basalt	<i>fine</i>	6.6	4.8	61.1	6.8	11.3	1.8E-05	4.8E-04
		<i>coarse</i>	6.5	3.1	3.7	3.6	7.2	1.4E-05	4.6E-04
	Granodiorite	<i>fine</i>	6.3	1.4	37.0	1.4	0.5	1.7E-05	4.6E-04
		<i>coarse</i>	6.0	0.4	19.0	0.5	0.1	2.1E-05	4.7E-04
	Tonalite	<i>fine</i>	6.5	2.3	18.0	1.9	0.8	1.5E-05	4.5E-04
		<i>coarse</i>	6.6	3.2	8.7	1.1	0.7	1.7E-05	4.4E-04
Oxic Atmosphere	Flood Basalt	<i>fine</i>	7.2	4.0	12.0	11.1	10.2	6.6E-05	6.0E-04
		<i>coarse</i>	6.9	5.2	9.1	8.6	18.6	4.3E-05	4.9E-04
	Granodiorite	<i>fine</i>	7.2	10.3	109.0	9.3	1.2	2.7E-05	5.0E-04
		<i>coarse</i>	7.2	2.9	8.0	3.1	1.2	4.7E-05	5.8E-04
	Tonalite	<i>fine</i>	7.3	1.2	47.9	4.3	0.7	9.5E-05	5.3E-04
		<i>coarse</i>	7.1	1.1	4.1	1.0	0.5	5.4E-05	4.6E-04
<i>Time = 6 Months</i>									
Anoxic Atmosphere	Flood Basalt	<i>fine</i>	6.5	3.5	0.3	2.5	3.3	1.7E-05	4.1E-04
		<i>coarse</i>	6.3	3.0	0.3	1.8	3.0	1.6E-04	5.8E-04
	Granodiorite	<i>fine</i>	6.3	3.4	1.4	1.9	0.5	1.2E-04	4.0E-04
		<i>coarse</i>	6.3	1.0	0.6	0.7	0.2	2.5E-05	4.0E-04
	Tonalite	<i>fine</i>	6.3	3.4	1.6	1.8	0.8	2.7E-05	3.8E-04
		<i>coarse</i>	6.6	3.6	1.2	1.0	0.4	1.3E-05	3.8E-04
Oxic Atmosphere	Flood Basalt	<i>fine</i>	7.5	2.7	0.5	1.1	6.7	4.4E-05	6.3E-04
		<i>coarse</i>	7.5	3.1	0.6	1.9	6.9	2.4E-05	4.5E-04
	Granodiorite	<i>fine</i>	7.7	3.1	10.3	2.1	0.7	2.8E-05	4.7E-04
		<i>coarse</i>	7.4	2.7	6.9	1.2	0.5	1.9E-05	4.6E-04
	Tonalite	<i>fine</i>	8.8	3.3	1.8	1.2	0.7	2.5E-04	7.3E-04
		<i>coarse</i>	7.4	1.2	0.6	0.3	0.2	5.0E-05	5.2E-04
<i>Time = 3 Months</i>									
Anoxic Atmosphere	Flood Basalt	<i>fine</i>	6.2	0.8	0.3	1.2	0.6	1.7E-05	4.1E-04
		<i>coarse</i>	6.4	0.7	0.2	0.9	0.6	1.6E-04	5.8E-04
	Granodiorite	<i>fine</i>	5.6	1.0	1.0	1.2	0.2	1.2E-04	4.0E-04
		<i>coarse</i>	6.3	0.5	1.1	0.9	0.1	2.5E-05	4.0E-04
	Tonalite	<i>fine</i>	5.9	0.7	0.7	1.8	0.1	2.7E-05	3.8E-04
		<i>coarse</i>	6.2	0.8	0.7	0.5	0.1	1.3E-05	3.8E-04
Oxic Atmosphere	Flood Basalt	<i>fine</i>	5.9	2.4	0.4	1.5	2.3	4.4E-05	6.3E-04
		<i>coarse</i>	6.1	2.7	0.3	1.6	2.7	2.4E-05	4.5E-04
	Granodiorite	<i>fine</i>	6.1	1.1	1.0	0.7	0.3	2.8E-05	4.7E-04
		<i>coarse</i>	5.9	1.6	0.9	0.7	0.3	1.9E-05	4.6E-04
	Tonalite	<i>fine</i>	5.8	0.8	0.4	0.6	0.3	2.5E-04	7.3E-04
		<i>coarse</i>	5.9	2.4	0.4	0.3	0.5	5.0E-05	5.2E-04
<i>Monitor Time = 12 Months</i>									
Present Atmosphere	Flood Basalt	<i>fine</i>	7.6	0.7	0.3	1.5	0.7	1.7E-05	4.2E-04
		<i>coarse</i>	7.1	0.7	0.2	0.4	0.8	1.2E-05	4.0E-04
	Granodiorite	<i>fine</i>	7.9	0.2	0.9	0.7	0.0	6.9E-05	5.6E-04
		<i>coarse</i>	7.7	0.2	0.8	0.7	0.0	1.3E-05	4.2E-04
	Tonalite	<i>fine</i>	7.7	0.8	0.3	0.1	0.0	9.8E-06	3.7E-04
		<i>coarse</i>	7.7	0.9	0.4	0.6	0.0	2.0E-05	5.5E-04

^aAll concentrations are expressed in mmol/L, only major species are depicted (with the exception of Fe and Al).

^bAlk refers to carbonate alkalinity namely [HCO₃⁻], calculated with electric balance in mmol/L. Note that anions species are not depicted in the table.

slightly higher for oxic experiments than for anoxic experiments, but without significant geochemical consequences. Likewise, microscopic observations of the altered grains do not show any significant differences between oxic and anoxic conditions

(Figure 2b). Consequently, the next section gives details about the second series of experiments (anoxic only), for which more data are available.

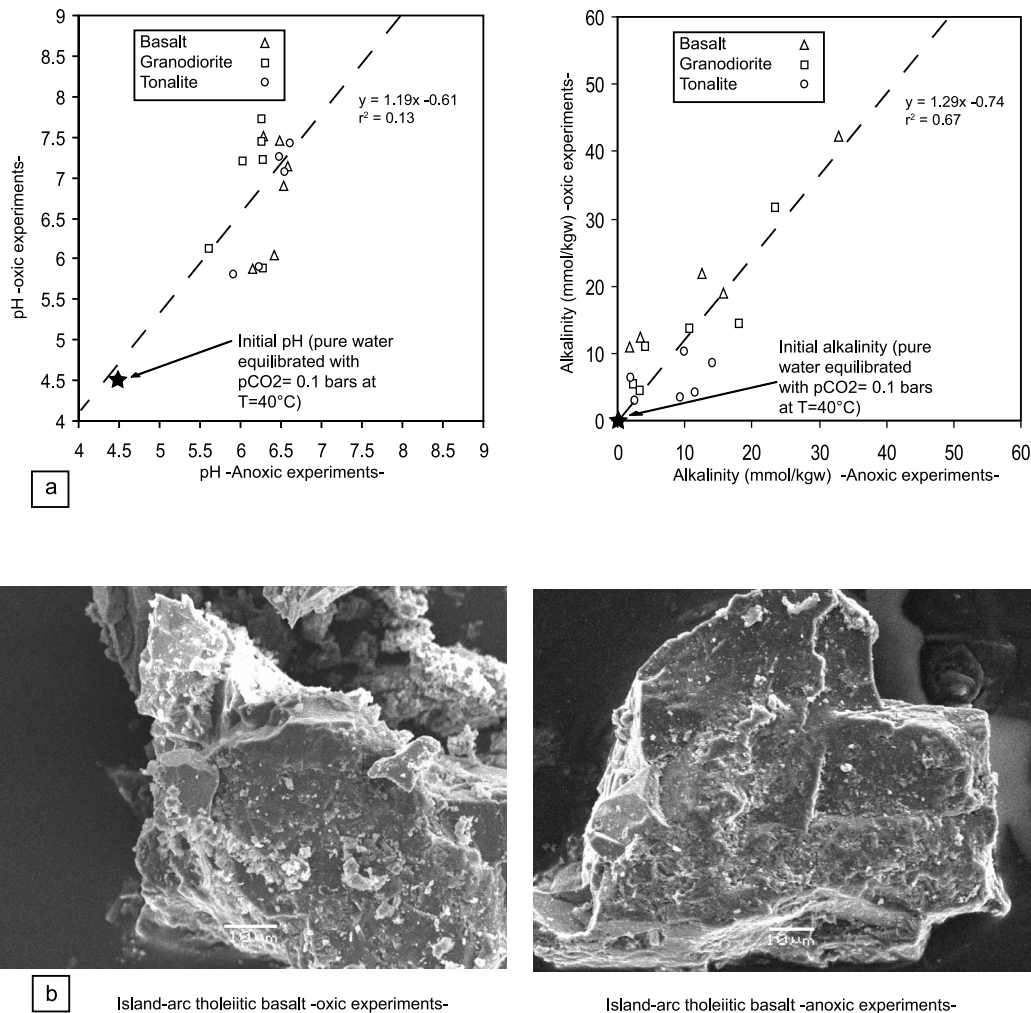


Figure 2. (a) Comparison of the pH (left side) and the alkalinity (right side) of the rock leachates in oxic and anoxic conditions (W/R = 1 and 5). Dashed line stands for the linear regression. (b) SEM photography (*Secondary Electron Imaging*) of primary mineral-plagioclase in island arc tholeiitic basalt in this case- at the end of the 1 yearlong experiments for the oxic (left side) and anoxic (right side) experiments. Secondary-phases deposits are clearly visible on the minerals surfaces.

4.2 Leaching Under Anoxic Conditions and W/R = 70

[24] The chemical compositions of the solutions are reported in Table 3b. It should be noted that, despite the duration, temperature and high CO₂ content of the experimental atmosphere, there is only a rather limited production of dissolved salts, with a total amount no higher than in natural mineralised water as shown on Figure 3. After a few weeks, the pH, alkalinity and almost all the ionic concentrations tend toward a stable value.

[25] The relative mobility of the elements was investigated by calculating a water/rock concentration ratio, according to *Gislason et al.* [1996],

which is normalized to sodium as shown below for element “X”:

$$R_{\text{mobility}_X} = (X_{\text{water}}/Na_{\text{water}})/(X_{\text{rock}}/Na_{\text{rock}})$$

where Na_{water} and X_{water} are the concentrations of Na and X in the solution; X_{rock} and Na_{rock} are the concentrations of X and Na in unaltered rocks. Sodium is chosen as a reference element here, since it is one of the most mobile ions in the three rock-types studied here, and occurs as a major element in rocks and water. Figure 4 shows the mobility of the elements relative to sodium.

[26] Iron and aluminum are the least mobile elements in all cases with R values less than 0.02. For

Table 3b (Sample). Experimental Results for the Second Set of Experiments^a [The full Table 3b is available in the HTML version of this article]

	Time	Sample	pH	Ca ²⁺	K ⁺	Na ⁺	Mg ²⁺	Fe ²⁺	Al ³⁺
Anoxic Atmosphere	5 days	<i>Flood Basalt</i>	5.63	MS	MS	MS	MS	MS	MS
		<i>Granodiorite</i>	4.99	MS	MS	MS	MS	MS	MS
		<i>Tonalite</i>	5.03	MS	MS	MS	MS	MS	MS
	15 days	<i>Flood Basalt</i>	5,93	0.10	0.50	0.06	0.20	1.1E-04	6.3E-04
		<i>Granodiorite</i>	5,4	0.02	0.10	0.01	0.01	2.3E-04	5.3E-04
		<i>Tonalite</i>	5,63	0.06	0.13	0.01	0.02	7.5E-05	4.6E-04
	30 days	<i>Flood Basalt</i>	5,95	0.12	0.43	0.06	0.20	2.4E-05	4.6E-04
		<i>Granodiorite</i>	5,47	0.02	0.12	0.01	0.01	1.2E-04	4.8E-04
		<i>Tonalite</i>	5,84	0.07	0.13	0.01	0.02	2.4E-05	4.6E-04
	45 days	<i>Flood Basalt</i>	6	0.12	0.20	0.07	0.20	3.9E-05	5.1E-04
		<i>Granodiorite</i>	5,67	0.02	0.13	0.01	0.01	4.4E-05	4.7E-04
		<i>Tonalite</i>	5,82	0.07	0.15	0.01	0.02	2.4E-05	4.6E-04
	60 days	<i>Flood Basalt</i>	6,05	0.13	0.21	0.07	0.20	4.4E-05	5.1E-04
		<i>Granodiorite</i>	5,63	0.02	0.13	0.01	0.01	9.2E-05	6.0E-04
		<i>Tonalite</i>	5,81	0.08	0.17	0.01	0.02	5.7E-05	4.8E-04
90 days	<i>Flood Basalt</i>	6,26	0.14	0.29	0.10	0.22	6.5E-05	5.4E-04	
	<i>Granodiorite</i>	5,87	0.02	0.13	0.02	0.01	7.3E-05	5.5E-04	
	<i>Tonalite</i>	6,03	0.08	0.17	0.01	0.02	5.9E-05	5.1E-04	
150 days	<i>Flood Basalt</i>	6,36	0.12	0.41	0.11	0.18	6.4E-05	5.1E-04	
	<i>Granodiorite</i>	6,27	0.03	0.20	0.02	0.01	5.9E-05	4.9E-04	
	<i>Tonalite</i>	6,29	0.13	0.20	0.02	0.03	6.2E-05	4.9E-04	
Present Atmosphere	150 days	<i>Flood Basalt</i>	7.2	0.04	0.06	0.01	0.04	2.5E-05	4.9E-04
		<i>Granodiorite</i>	7.25	0.02	0.17	0.02	0.01	2.5E-05	4.9E-04
		<i>Tonalite</i>	7.06	0.05	0.18	0.02	0.01	2.1E-05	4.6E-04

^aAll concentrations are expressed in mmol/L, only major species are depicted (with the exception of Fe and Al). Alk refers to carbonate alkalinity namely $[\text{HCO}_3^-]$, calculated with electric balance in mmol/L. Note that anions species are not depicted in the table. MS: monitoring of the solutions, pH and Eh measurements only without sampling.

the other elements, the relative mobility varies depending on rock type with an increase of R from basalt to tonalite. These high values suggest that Na, our reference, is less mobile in tonalite than basalt, according to the lower reactivity of Na-plagioclases than Ca-plagioclases (basalt). In the granodiorite leachate, concentrations are very low and the mobility of the elements is reduced, granodiorite being the least weatherable among the tested rocks.

[27] Field studies on basalts have shown almost the same sequence of relative mobility of the elements: for example, *Veldkamp and Jongman* [1990] give a decreasing order of mobility for basalts in France, with $\text{K} > \text{Na} > \text{Si} > \text{Mg} > \text{Ca} > \text{Al} > \text{Ti}$.

4.3. Development of Secondary Phases

[28] Figure 5 reports the mass of secondary phases, corresponding to the fine particles released by ultrasonic treatment, which show a regular and weak increase with time for the three types of rocks. The mass of newly formed phases at the end of the experiment is nearly 10^{-3} g for the basalt and less than half that value for the two other rocks (Figure 5) (respectively 1% and 0.5% of the initial mass of ca 0.1 g).

[29] EDS analyses suggest an Al-Fe-Si rich composition for the secondary phases. However, these chemical data should be interpreted with caution since the bulk composition of the fine particles could be affected by mixing with primary minerals. XRD patterns obtained from the recovered ultrasonic fraction show a sharp peak at 10 Å for the granodiorite and tonalite products, likely related to contamination of this fraction by primary micaceous phases. Except for this artifact, we only distinguished a broad peak around 14 Å (see Figure 6), supporting the hypothesis of a poor degree of crystallization of the secondary phases.

[30] X-ray diffraction failed to establish the presence of any carbonate minerals. The absence of carbonate is also supported by the fluid chemistry. For each sampled solution, we calculate the saturation state of the fluid with respect to the potential secondary phases using the PHREEQC software (*Appelo and Parkhurst* [1999]; see section 5 for more detailed information). The saturation state is quantified by the saturation index $(\text{SI})_i$ for a solid phase i and expressed in the following form:

$$(\text{SI})_i = \log\left(\frac{\text{IAP}}{K_i}\right) \quad (1)$$

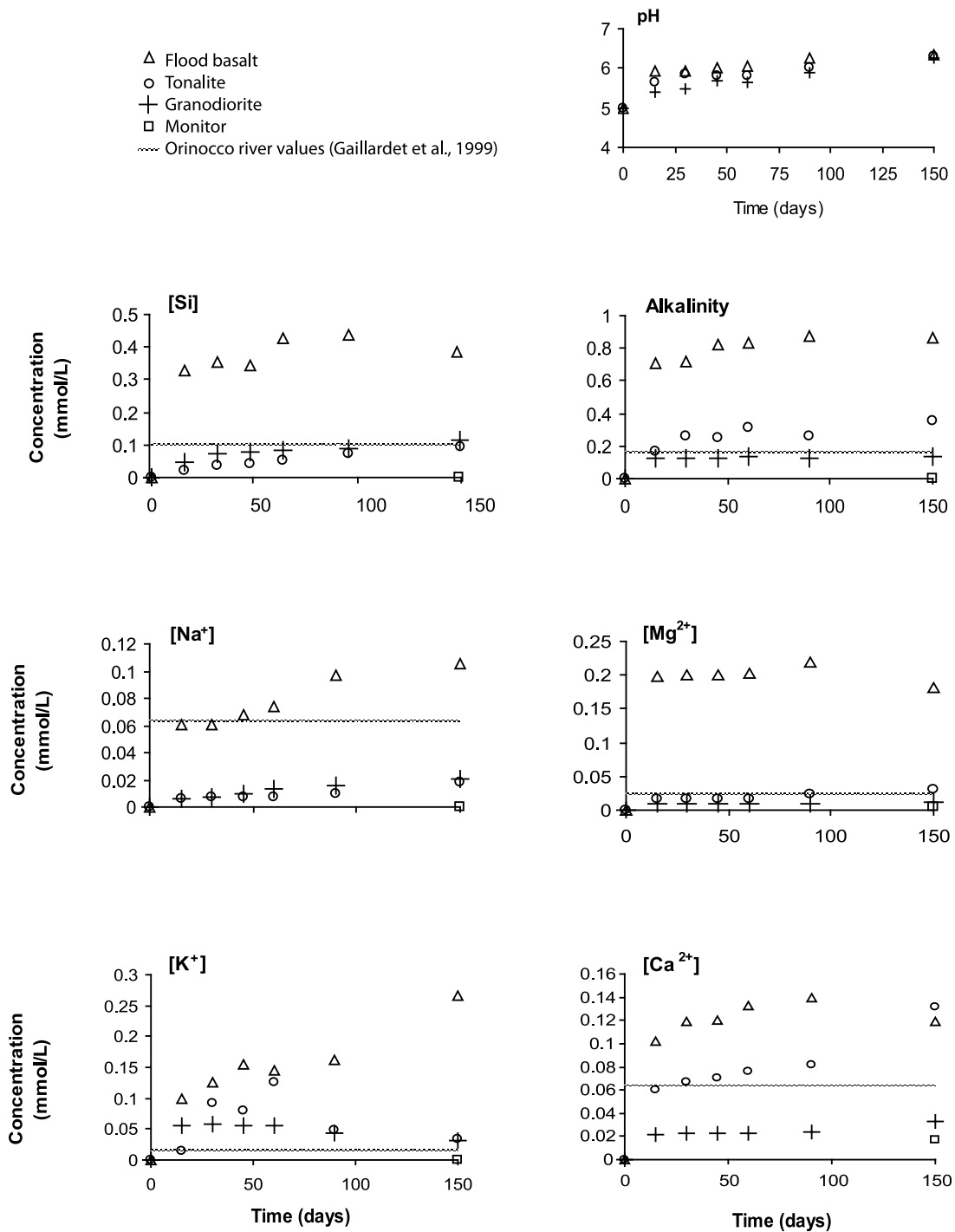


Figure 3. Evolution of the chemical composition of the solutions during the flood basalt (triangles), granodiorite (crosses) and tonalite (circles) weathering for $p\text{CO}_2 = 0.1$ bars, and $T = 40^\circ\text{C}$ compared with Orinoco River values (discontinuous lines) (after Gaillardet et al. [1999]), chosen as a representative terrestrial river ($125\text{--}500 \mu\text{m}$, $W/R = 70$).

where IAP is the Ionic Activity Product and K_i the thermodynamic equilibrium constant. At equilibrium, $(SI)_i$ is equal to zero, but is positive in supersaturated solution and negative in undersaturated solution. The results of the calculations presented in

Table 3b display negative saturation index for carbonate minerals. However, in the first series conducted for 1 year, $(SI)_i$ reached positive values at the end of the runs, but no carbonate mineral was ever found. The absence of observed carbonate in these

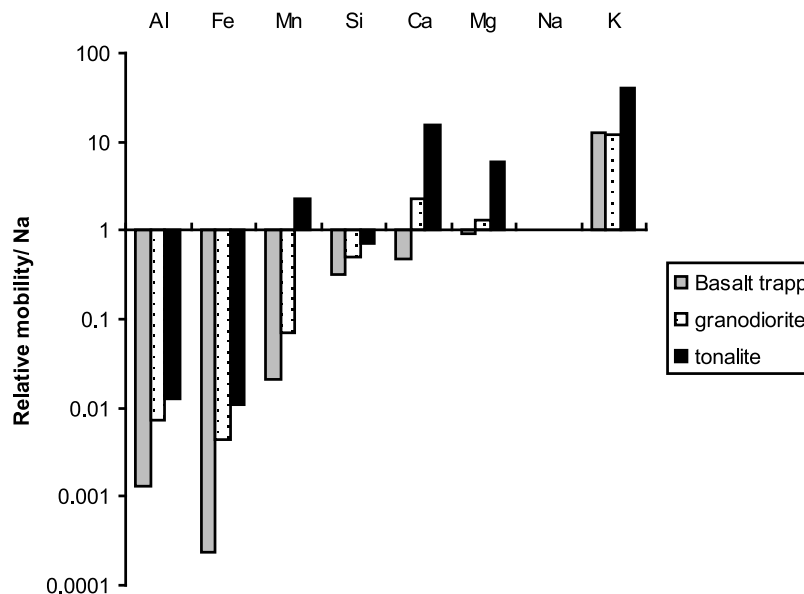


Figure 4. Relative mobility of some elements during the weathering of flood basalt (black line), granodiorite (white) and tonalite (gray) for 5 months of experiment. (Duration 5 months, coarse grains, W/R = 70).

long runs may be related to the possible poor crystallinity of the secondary phases or their very low concentration if present. This makes it questionable to use XRD for identifying small amount of carbonate. In addition, products of the longer runs were analyzed by Fourier Transform Infrared Spectroscopy (FT-IR). The analyses were carried out on a Nicolet 510 spectrometer (HydrASA Poitiers University, France) and failed to identify secondary carbonates. The details of the method and examples of application can be found elsewhere [Petit, 2006; Andrieux and Petit, 2010; Vingiani et al., 2010].

[31] The absence of carbonate as by-product of silicates alteration under high $p\text{CO}_2$ indicates that the progress of reaction was not long enough to allow the rock samples to buffer the solution pH.

4.4. Changes of Primary Mineral Surfaces

[32] At the end of the experiments, the altered samples were cleaned by ultra-sonic treatment, air-dried and then observed using scanning electronic microscopy (SEM). First, we note that each grain is formed of several mineral species. Observed under SEM, the altered surfaces appear different from one rock to another, with the granodiorite being less altered than the basalt and the tonalite, according to the recovered mass of fine particles. In Figure 7, cleaned surfaces are shown on the left and altered grains on the right.

[33] In the case of basalt (Figures 7a and 7b), the only observable alteration feature is made up of

dissolution pits in the cryptocrystalline matrix, while pyroxene phenocrysts seem well preserved. By contrast, the pyroxene phenocrysts from the altered tonalite (Figures 7c to 7f) show rough and damaged surfaces with remaining small particles.

[34] Figures 7g and 7h display alkali-feldspar surfaces in altered/fresh granodiorite samples. No clear sign of alteration can be observed.

[35] Several clay minerals (kaolinite, Mg- and Ca-montmorillonite, see Table 3b) are already supersaturated with respect to the fluid in the first samples collected, whereas the precipitation of carbonates remains thermodynamically disfavored throughout the duration of the experiments.

5. Construction and Validation of the Numerical Model

[36] The aim of our numerical approach is to parameterize a simple model, including an empirical variable to fit the experimental results, so that the model can be extrapolated to the geological scale. For this purpose, we chose to use the PHREEQC program [Appelo and Parkhurst, 1999] developed by the U.S. Geological Survey for modeling water-rock interactions, coupled with the Lawrence Livermore National Laboratory database. The program determines the chemical speciation of aqueous solutes, the fugacities of gases, and attributes each component of the solution to stable aqueous species. It also calculates the activity

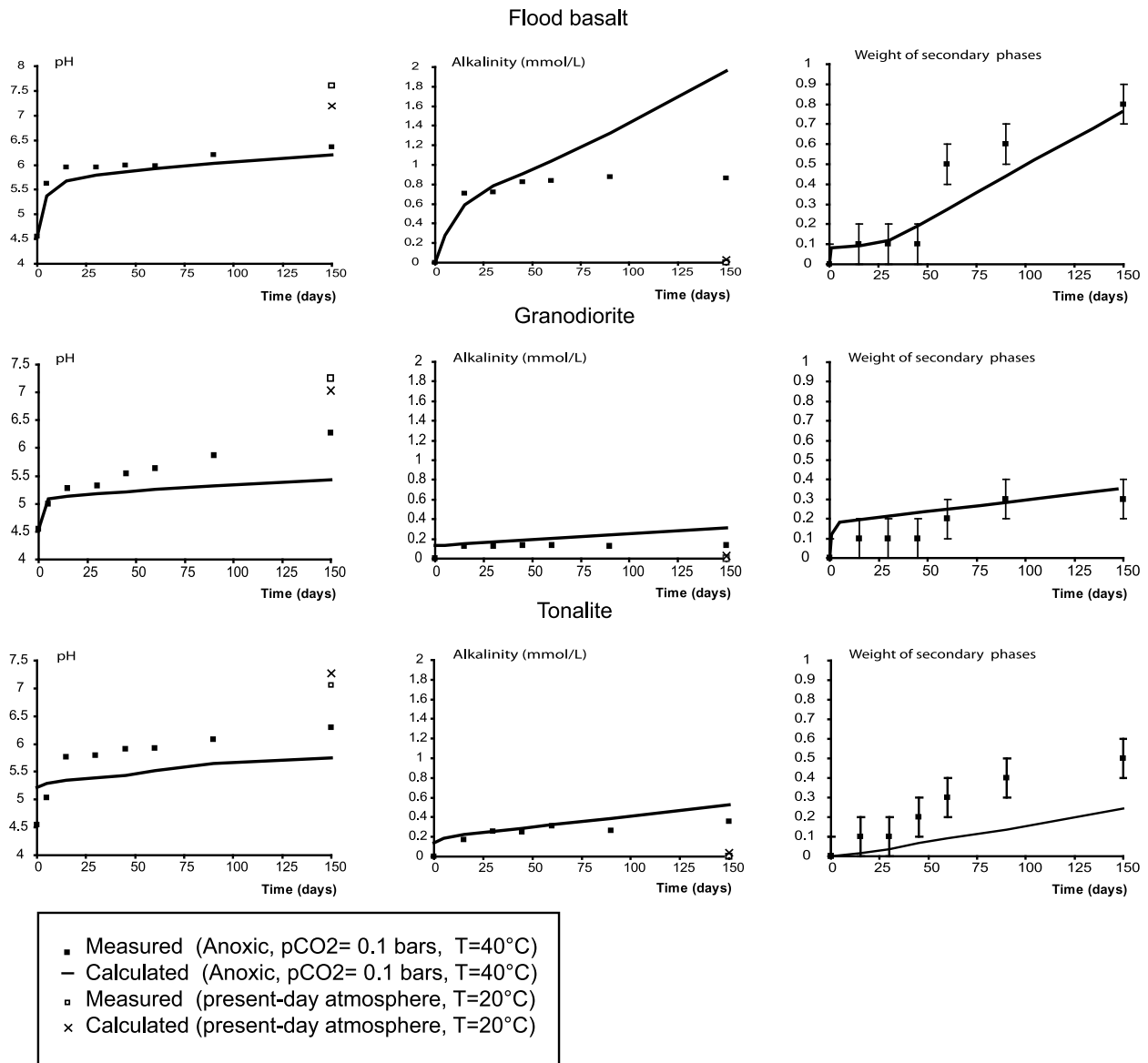


Figure 5. (top) Flood basalt, (middle) granodiorite, and (bottom) tonalite. Extensive and intensive parameters chosen in order to calibrate the numerical model: pH, alkalinity and weight of the secondary phases. (Duration 5 months, coarse grains, W/R = 70).

coefficients of water and the aqueous species, as well as the saturation index of the solution with respect to all the solid phases of the database.

5.1. Parameters of the Model

[37] The mineral dissolution rate is described in the model by a first-order kinetic law for a surface-controlled reaction. More elaborate formalisms have been proposed in the literature [Schott and Oelkers, 1993; Oelkers et al., 1994, Oelkers and Gislason, 2001] including the catalytic Al inhibition effect according to the Al concentration. How-

ever, (1) the fluid data presented here indicate that the leachate remains far from equilibrium, as shown in Table 3a, with respect to the rock-forming minerals of the altered samples and (2) the Al concentrations are very low. Finally, we adopt a simpler approach that consists of modeling the dissolution rates with a basic first-order law reported in equation (2):

$$R_i = \left(\frac{dn}{dt}\right) = r_i \frac{A}{V} \left(1 - \frac{IAP}{K_i}\right) \quad (2)$$

where R_i stands for the bulk dissolution rate of mineral i , r_i is the dissolution rate constant in mol/m²/s,

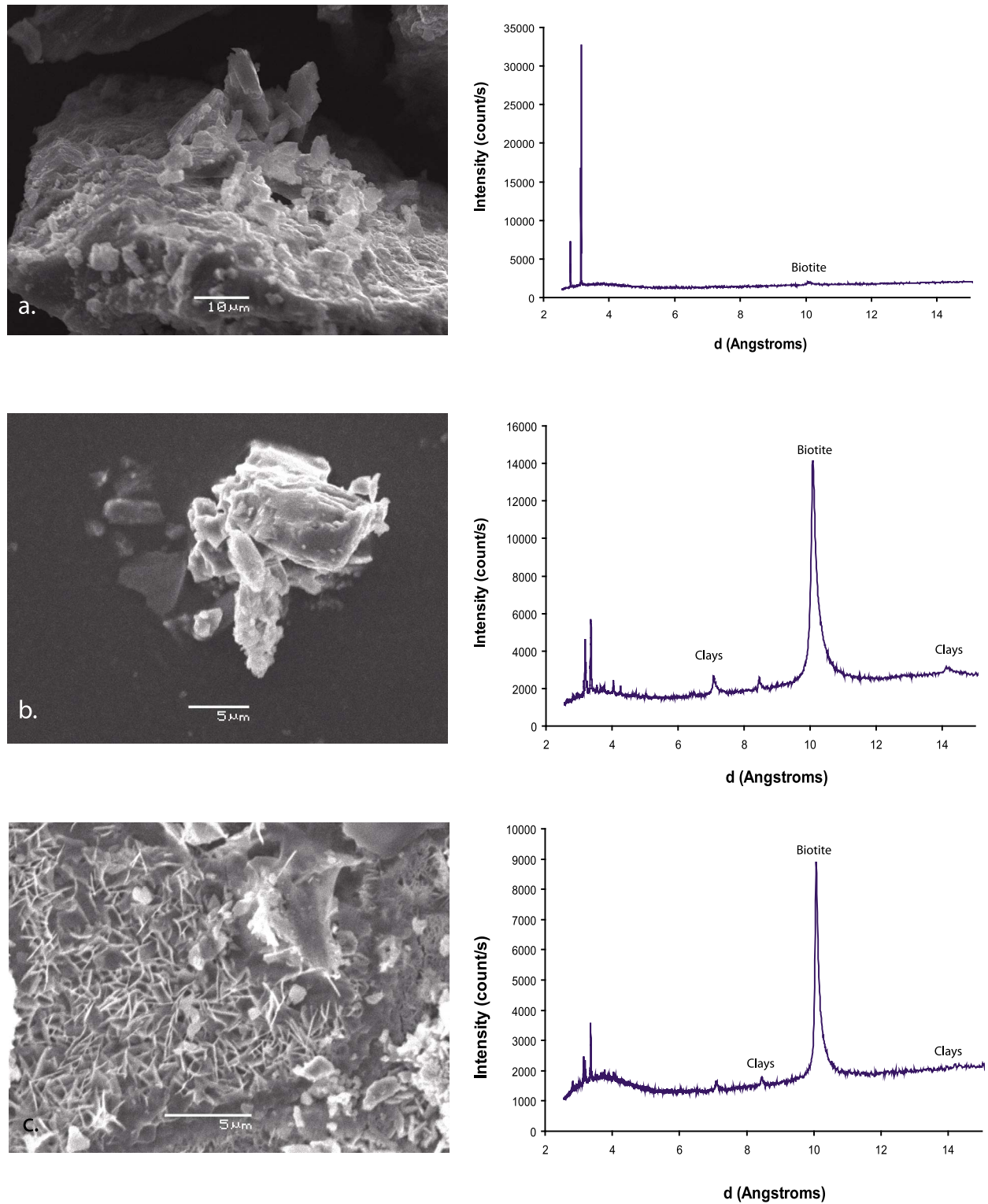


Figure 6. To the left, SEM morphology of the secondary alteration phases at the surface of (a) basalt, (b) granodiorite and (c) tonalite grains. To the right, corresponding XRD spectrums of the “purified” secondary minerals (duration 5 months, coarse grains, W/R = 70).

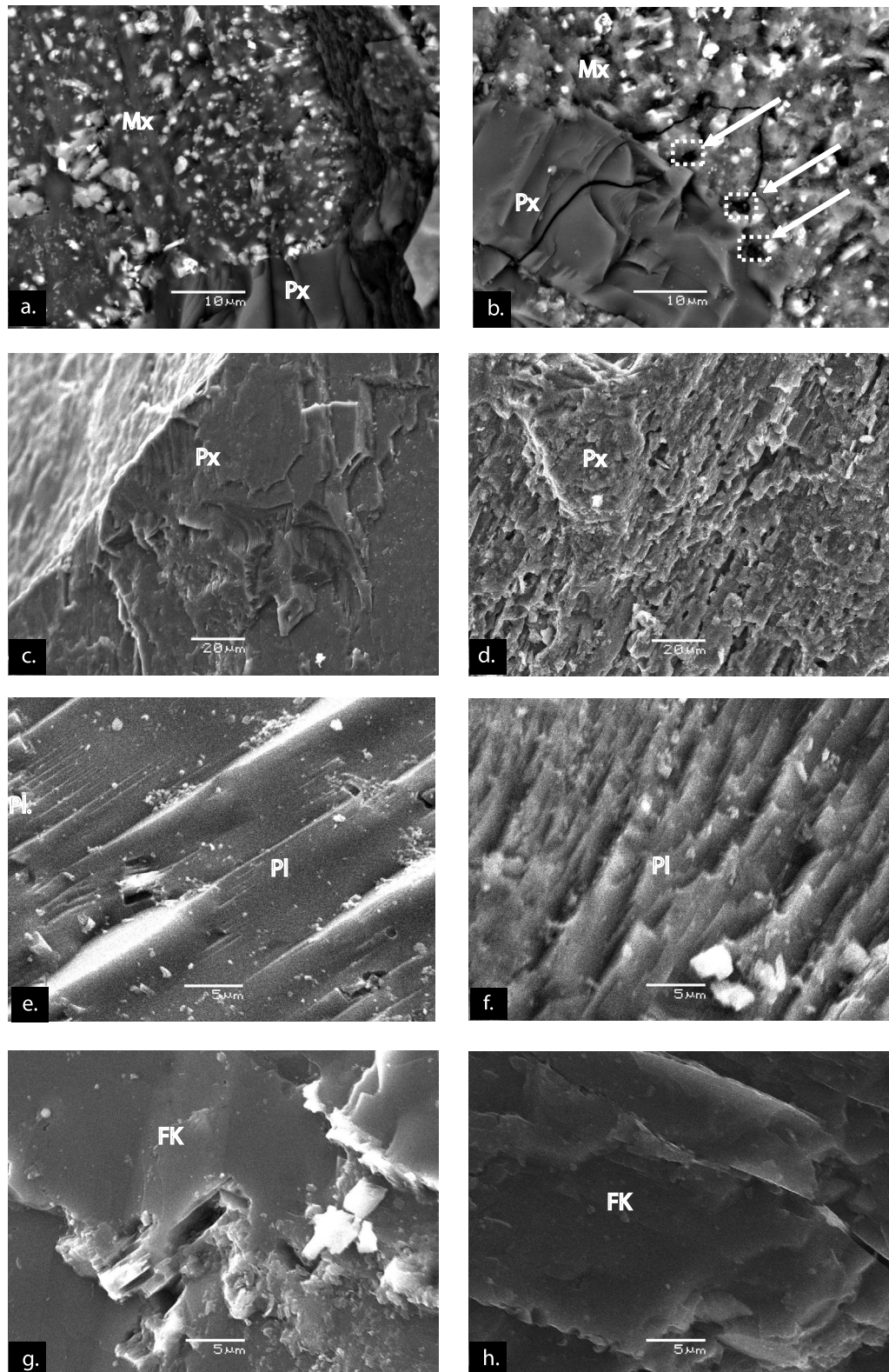


Figure 7. SEM (*Backscattered electrons*) photographs of unaltered (left column) and altered (right column) powder after 5 month experiment (125–500 μm , W/R = 70)) ((a, b) basalt; (c, d, e, f) tonalite; (g, h) Granodiorite). Pl: plagioclase, Px: pyroxene, Mx = cryptocrystalline matrix, FK = orthose.

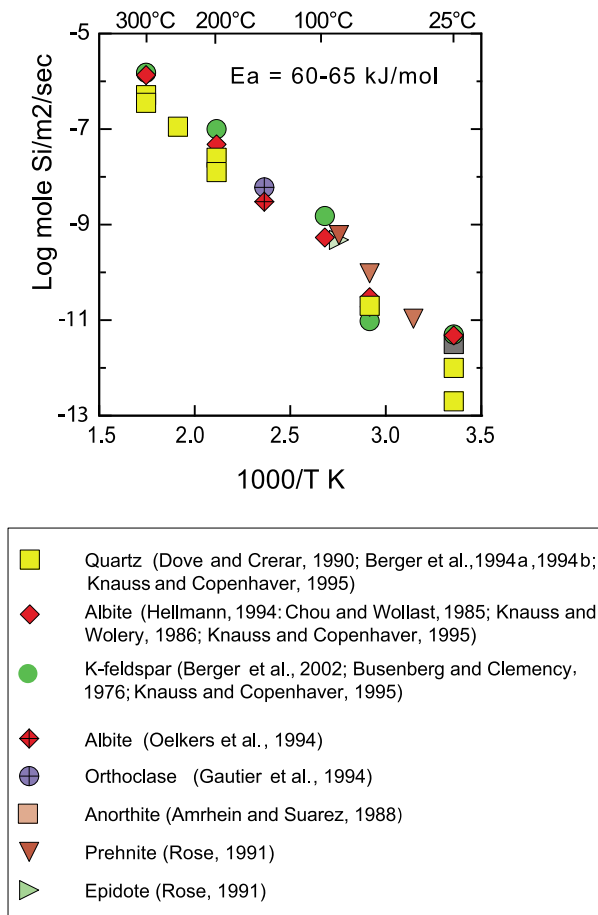


Figure 8. Arrhenius plot of the dissolution rate constants of tetraoxosilicates at neutral pH or when the hydrolysis of silica is the limiting step (after *Berger et al.* [2002]).

A is the surface area of the mineral, V is the volume of the solution.

[38] To determine the rate constants, we use the approach reported by *Berger et al.* [2002], which consists of relating the bulk dissolution rate to the silica concentration in the mineral at near neutral pH (Figure 8). This approach is applied here to the entire set of minerals of used in the modeling study, and the rate constant database is calculated from a simple function relating temperature with Si content of the dissolving mineral (see Table 4 and Appendix A).

[39] The reactive surface is initially assumed to be equal to the mineral surface-area measured by BET. For the granodiorite and tonalite, the values are close to $0.2 \text{ m}^2 \cdot \text{g}^{-1}$ (Table 2). In the case of the flood basalt, the measured BET surface is much higher than for the two other rocks, probably because a substantial part of the BET surface corresponds to the cryptocrystalline matrix (our SEM observations

and *Scopel* [1997]). The crystallinity of the basaltic flow and the reactivity of the glass fraction (if any) is an important point for our modeling. However, for the purpose of our study, we consider that sub-aerial flood basalts produced massive lava flows. The glass in such lava flows is absent or rare (and restricted to the quenched border). In fact, the rock matrix of the studied sample contains microlites and abundant cryptocrystalline phases (oxides, plagioclase, pyroxene and clays, identified by SEM), according to the petrographic description presented in section 2.

[40] We can raise the question of how this clay fraction could contribute significantly to the weathering budget, even when it represents only at few percent of the whole rock. First, this clay fraction was probably formed by volcanic gas-rock interactions just after solidification of the lava flow [*Meunier et al.*, 2008, and reference therein], and thus did not result from a weathering process (i.e., did not consume atmospheric CO_2). Second, even considering subsequent weathering, clay minerals are more stable than mafic minerals at the Earth's surface. A simple mass bal-

Table 4. Rate Constants Used in the Numerical Modeling per Minerals and per Type of Rock and Experimental Conditions^a

	k_0 (T= 40°C) in mole Si.m ² .s ⁻¹	Experimental Conditions (A/V in m ² .kg ⁻¹)
<i>Basalt</i>		
Albite	3.3E-12	13
Anorthite	5.0E-12	12
K-feldspar	3.3E-12	4
Diopside	1.0E-11	11
Hedenbergite	1.0E-11	10
Ilmenite	6.1E-10	3
Magnetite	1.7E-08	0.1
<i>Granodiorite</i>		
Quartz	1.0E-11	0.7
Albite	3.3E-12	0.7
Anorthite	5.0E-12	0.5
Orthose	3.3E-12	0.4
Phlogopite	3.3E-12	0.1
Annite	1.3E-12	0.2
<i>Tonalite</i>		
Quartz	1.0E-11	0.6
Albite	3.3E-12	0.7
Anorthite	5.0E-12	0.3
K-feldspar	3.3E-12	0.0
Phlogopite	3.3E-12	0.2
Annite	3.3E-12	0.2
Amphibole	1.3E-12	0.1
Diopside	1.0E-11	0.2
Hedenbergite	1.0E-11	0.1

^a*Berger et al.* [2002]. The overall reaction is controlled by silica hydrolysis.

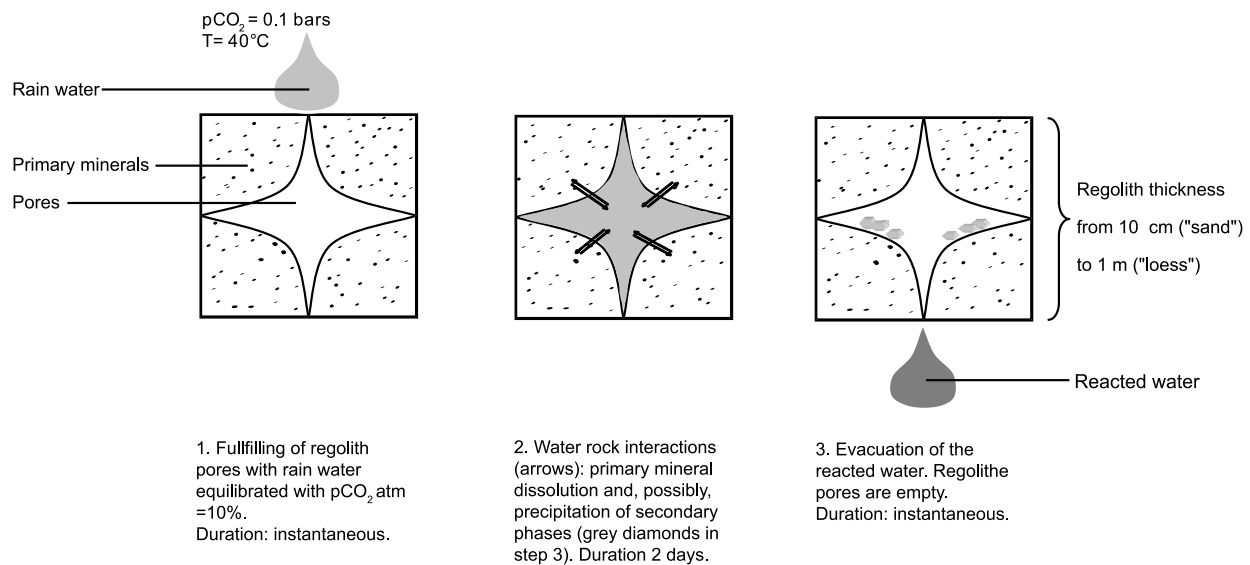


Figure 9. Conceptual steps of the “Pulse-Chase” modeling of the water-rock interactions, at the microscopic scale, between two rain events.

ance equation of smectite dissolution indicates half of the proton-consumption ($16 \text{ H}^+/\text{kg}$) when compared to plagioclase hydrolysis ($29 \text{ H}^+/\text{kg}$). Consequently, this fraction is ignored in our calculation.

[41] It is difficult to estimate the reactive surface area for the plagioclase and pyroxene microcrysts, even if their dissolution rate constant is probably the same as the phenocrysts. Our experiments yield roughly similar alteration rates for basalt (micro-litic) as the two other rock samples (granular). This unexpected observation leads us to conclude that the fine mineral fraction is less reactive than the coarse fraction (e.g., lower water accessibility?). We consider that the BET-measured value may be inappropriate, so we only take into account the surface area of the phenocryst fraction. For basalt, this phenocryst fraction is assumed to be roughly equal to that observed in the other rocks.

[42] For each rock sample, we use the whole-rock analysis and image analysis to calculate the modal percentage of each mineral species (Table 2). The two methods provide consistent modal compositions. These mineral compositions are used to divide up the whole surface area (i.e., measured by BET) into a specific reactive area for each mineral constituent according to its modal percentage (see Table 2).

[43] The dimensioning of the other parameters (water-rock ratio, $p\text{CO}_2$, gas-water volume ratio, temperature and duration) reproduces the experimental conditions.

[44] In our simplified approach, the secondary phases are allowed to precipitate as soon as their SI

value is positive and without any explicit kinetic law. As a result, the overall alteration rate is mainly controlled by the dissolution kinetics of the primary mineral constituents. This assumption is supported by the low SI value of the primary minerals measured in the experiments (Table 3). Among all the potential secondary phases, we exclude the mafic minerals (feldspar, pyroxene, etc.) and quartz, whose precipitation rate is well known to be extremely slow at 40°C .

5.2. Preliminary Results and Model Adjustment

[45] Experimental and calculated data are compared by means of intensive and extensive parameters (pH, HCO_3^- taken as alkalinity, and mass of secondary phases).

[46] The two sets of data display a radically different behavior with time: the calculated data show a linear progression with time, whereas the experimental data show an inflection point between the 5th and the 15th day (especially for the pH and alkalinity, see Figure 5). This allows us to distinguish two steps during the mineral weathering: (1) “initial dissolution” corresponding to the fast dissolution of the fresh grain surfaces; and (2) a more gradual dissolution reaction, subsequently referred to below as “further dissolution.”

[47] The “initial dissolution” stage is reproduced in our model by introducing the immediate dissolution of a mineral layer without any kinetic law, followed by the “further dissolution” regime modeled by the

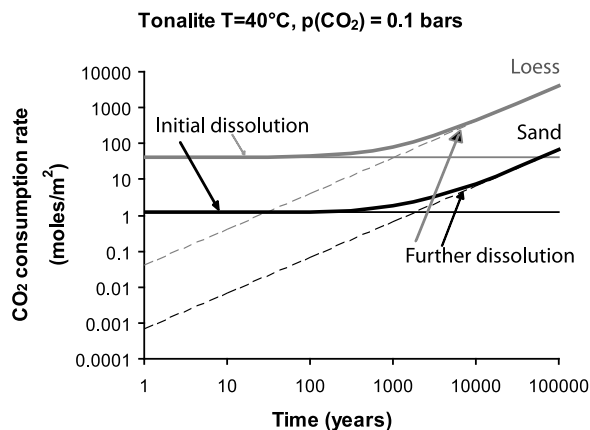


Figure 10. CO_2 consumption rates in the case of loess (gray line) and sand (black line). Batch dissolution resulting from initial fresh surface and further dissolution are displayed separately respectively with solid and dashed lines. The sum of the two effects is also displayed (solid curves).

previously defined kinetic parameters. A calculation using the PHREEQC software [Appelo and Parkhurst, 1999] yields a value for this exchange layer. The input solution is assumed to be pure water equilibrated with an atmosphere containing 10% CO_2 . The amount of dissolved mineral during this stage is chosen to fit the experimental data and correspond to a thickness of $0.5 \mu\text{m}$ for the dissolved layer. In fact, this value is the only adjusted parameter of the model. Overall, the model satisfactorily reproduces the experiments, even though some discrepancies can be observed (Figure 5) between the modeled and observed values, as for example, in the granodiorite leachates, where we find a difference of one pH unit.

[48] Moreover, we also make use of the data from the monitor runs corresponding to present-day weathering conditions, namely $p\text{CO}_2 = 10^{-3.5}$ bars and $T = 20^\circ\text{C}$. Given the low carbon dioxide pressure, we set the leached layer thickness to zero. Again, we find a reasonably good agreement between the calculated and measured chemical evolution.

5.3. “Scaling up” to Precambrian Earth

[49] The previous calibrated formalism based on two concomitant reactions is used to model the weathering of the continental surface under Precambrian conditions.

[50] The “rock” is a regolith of variable grain size and thickness, reacted with rainwater initially equilibrated at 40°C with $p\text{CO}_2 = 0.1$ bars, under anoxic atmosphere. The drainage conditions are

arbitrarily fixed to three rainy days per week. The consumption of atmospheric CO_2 as a consequence of mineral weathering is simulated as a function of time by an incremental procedure and used to recalculate the temperature and dissolution rate constants at each step. The regolith alteration is assumed to proceed by a continuous batch process in a saturated sediment whose pore water is periodically renewed at each rain event. The water-rock ratio between the rain falls is defined by the porosity of the regolith, that is, for a compact sphere model, roughly $0.2 \text{ m}^3 \text{ water/m}^3$ of regolith (values from Fetter [1994] for a glacial tillite). At each rainfall, the pore filling water is replaced by an equivalent volume of fresh rainwater. The procedure is detailed in the appendix below and illustrated in Figure 9.

[51] Among all results, we focus on the CO_2 consumption rate. The first step of dissolution (exchange reaction) is clearly the more important contribution relative to the CO_2 consumption, at least over the first 1,000 yrs for the sand and 1,850 yrs for the loess (Figure 10).

[52] In our model, grain-size is the major factor influencing the CO_2 -consumption rate (Figure 10). The two extreme studied cases show contrasted results: for the fine grain-sized material – i.e., “loess” – the CO_2 consumption rate is nearly two orders of magnitude faster than for the coarse grain-sized material – i.e., “sand.” This parameter seems to be crucial for CO_2 consumption during rock weathering, because it determines the reactive surface of the minerals. In the simulations, only carbonates (namely, calcite and disordered dolomite) are allowed to precipitate. Only the first stage (i.e., exchange reaction followed by dissolution after the first rain event) enables to reach positive saturation index, and this occurs only for calcite. After the rain event, the pore filling solution never exhibits carbonate precipitation.

6. Discussion

6.1 Comparison With Natural Data

[53] To compare our experimental solutions with present-day rivers, Figure 3 reports the water chemistry for the Orinoco River, with a catchment including composite but moderately silicic lithologies [Gaillardet et al., 1999], which represents a benchmark among the least mineralised rivers of the world. As can be seen in Figure 3, the concentrations for granodiorite and tonalite leachates are very similar and systematically lower than the

concentrations found in this natural river. However, this is not the case for the basaltic leachates, where the pH values are in the same range for both experimental and natural waters.

6.2. Mechanism at the Interfaces

[54] The primary mineral dissolution rates can be correlated with the time-evolution of three parameters: the pH, the alkalinity and the mass of secondary phases (Figure 5). Two stages can be distinguished: a first stage occurring during the first five days, followed by a second stage of weaker intensity.

[55] The first stage corresponds to the development of a leached layer at the primary mineral surface. It consists of an exchange between protons of the solution and the network-modifying cations i.e., those that do not form part of the structural mineral framework. Typically, the thickness of the leached layer increases with time and decreasing pH, as shown for example by *White and Claasen* [1980] and *White* [1983]. These exchange reactions release cations and increase the solution pH as observed in our experiments. The depth of the cation-exchange layer has been measured by surface titration and may attain several tens of Å [*Amrhein and Suarez*, 1988, *Schweda*, 1989, *Blum and Lasaga*, 1991, *Wollast and Chou*, 1992]. In other words, the dissolution of a mineral layer about 5000 Å thick, leads to the pH and alkalinity values observed in the experiments. The thickness of the leached layer is within the range of classical values in the literature adopted for this type of experiment. As an example *Hamilton et al.* [2001] shown that a jadeite-glass dissolved at pH = 2 developed an Al-Na depleted surface that is thousands of Angstrom thick. The interesting point is that this value is the same for the three types of rocks.

[56] The second important aspect of weathering is the high pH buffering capacity of rocks, which balances the acidity of the atmosphere. However, the numerous experimental investigations of the effect of pH on silicate dissolution [e.g., *Brantley and Chen*, 1995; *Nagy*, 1995; *Blum and Stillings*, 1995] suggest that different silicate phases respond differently to pH variations. It is noteworthy that the polyminerale grains observed in our study give rise to an “average” dissolution rate for the rocks considered. As noted by several authors, the first exchange reaction is followed by a slower parabolic solid-state diffusion [*White and Claasen*, 1980; *White*, 1983]. The increasing aqueous pH leads to a

decrease in the rate constants of diffusing species that is proportional to their valence state. As a consequence, the diffusion gradients produced by solid-state internal exchange are weaker.

6.3. Consequences for Precambrian Times

[57] A comparison between experimental solution chemistry under “Precambrian conditions” ($p\text{CO}_2 = 0.1$ bars, $T = 40^\circ\text{C}$) and “Present-day conditions” ($p\text{CO}_2 = 10^{-3.5}$ bars, $T = 20^\circ\text{C}$) allows us to quantify the ratio between the corresponding weathering intensities. We focus on alkalinity here, assuming that this parameter is a good indicator of weathering intensity. The alkalinity ratios are comprised between 4 for granodiorite and 8 for tonalite, with an intermediate ratio for basalt (Table 3). This suggests that weathering under Precambrian conditions is 4 to 8 times more aggressive than in the modern Earth. A similar value (7 times) is found by *Higgins and Schrag* [2003], based on calculations carried out by L.R. Kump. An important difference with the Higgins and Schrag model is that these authors attribute a large part of the alkalinity to the dissolution of continental carbonates, whereas we obtain similar values by taking into account solely the silicate contribution.

[58] Among the different rocks occurring at the surface of the continents, basalts are regarded as the most easily weatherable on the present-day Earth, whatever the climatic conditions [*Gislason and Arnórsson*, 1993; *Gislason et al.*, 1996; *Whipkey et al.*, 2002; *Chadwick et al.*, 2003; *Sigfusson et al.*, 2006]. The field study of *Dessert et al.* [2003] and our experimental data both confirm the role of a CO_2 sink for this type of rock. For example, Figure 5 shows that the CO_2 consumption rate evaluated from the HCO_3^- concentrations is two times higher than for the two other types of rock.

7. Conclusions

[59] Experiments lasting several months to simulate the weathering of rock powders under $p\text{CO}_2 = 0.1$ bars and $T = 40^\circ\text{C}$ lead to mineralized solutions with pH close to neutrality and the formation of poorly crystallized secondary phases. These observations highlight the very high buffering capacity of the rocks; moreover, the intensity of the rock dissolution – in which each grain is polyminerale – depends on the crystallinity and the nature of the rock-forming minerals. As a result, the solution chemistry shows that, as classically expected, basalt is more easily weathered than

tonalite, which is more easily weathered than granodiorite.

[60] In detail, the results of this study show two characteristics of weathering under high $p\text{CO}_2$: (1) the importance of the first dissolution stage in the dissolution process and (2) the low overall alteration rate despite the CO_2 -rich atmosphere and high temperature of the experiments. In particular, the evolution of the alkalinity and of the pH seems to indicate that the mineral dissolution occurs in two stages or according to two exchange reactions. The first stage occurs during the five first days, followed by a second stage with slower dissolution.

[61] The innovation of our study is to introduce an empirical factor – the thickness of the leached layer – to fit the data, which is then used to construct a numerical model of rock weathering as described in the second part of the article.

[62] From our thermo-kinetic point of view, the intensity of Precambrian weathering under high $p\text{CO}_2$ conditions, especially in the immediate post-Snowball Earth aftermath, is more severe than at the present-day, up to 6 times more than currently observed on Earth. However, this is not as severe as might be considered appropriate for such high CO_2 pressure.

Appendix A: Numerical Modeling

[63] Table A1 shows parameter values chosen for simulations used with the numerical model in the case of the “Precambrian Earth.” Note that the terms “sand” and “loess” simply refer to two different grain-sizes and not to a mineralogical composition (see section 5.3 for further details). Table A2 shows rate constants [Berger *et al.*, 2002] used in the various modeling per minerals

Table A2. Rate Constants Used in the Various Modeling per Minerals and Type of Rock^a

	% of Mineral Surface	k_0 (T= 40°C) in mole $\text{Si.m}^2.\text{s}^{-1}$	Simulations (A/V in $\text{m}^2.\text{kg}^{-1}$)	
			Loess	Sand
<i>Basalt</i>				
Albite	23	3.3E-12	138	3
Anorthite	22	5.0E-12	132	3
K-feldspar	7	3.3E-12	42	1
Diopside	19	1.0E-11	114	3
Hedenbergite	18	1.0E-11	108	3
Ilmenite	6	6.1E-10	36	1
Magnetite	0.1	1.7E-08	1	0.02
<i>Granodiorite</i>				
Quartz	25	1.0E-11	135	3
Albite	25	3.3E-12	135	3
Anorthite	19	5.0E-12	103	3
Orthose	13	3.3E-12	70	2
Phlogopite	4	3.3E-12	22	0.5
Annite	8	1.3E-12	43	1
<i>Tonalite</i>				
Quartz	20	1.0E-11	135	3
Albite	29.8	3.3E-12	150	4
Anorthite	13.8	5.0E-12	58	1
K-feldspar	5	3.3E-12	6	0.2
Phlogopite	6.5	3.3E-12	46	1
Annite	5.5	3.3E-12	35	0.9
Amphibole	5	1.3E-12	27	0.7
Diopside	9	1.0E-11	49	1
Hedenbergite	5	1.0E-11	32	0.8

^aBerger *et al.* [2002]. Note that the terms “sand” and “loess” simply refer to two different grain-sizes and not to a mineralogical composition.

and type of rock (see sections 5.1 and 5.3 for further details).

Appendix B: Supplemental Chemical Data

[64] The pH and Eh (mV) measurement for the two sets of experiments: Table B1 refers to oxidic versus

Table A1. Parameters Values Chosen for Geologic Simulations Used With the Numerical Model^a

	Basalt		Granodiorite		Tonalite	
	Loess	Sand	Loess	Sand	Loess	Sand
Density of soil	3	3	2.7	2.7	2.7	2.7
Grain-size (mm)	50	2000	50	2000	50	2000
Thickness of soil (m)	1	0.1	1	0.1	1	0.1
Specific surface ($\text{m}^2.\text{kg}_{\text{soil}}^{-1}$)	0.04	0.001	0.04	0.001	0.04	0.001
Porosity (%)	20	20	20	20	20	20
A/V: Reactive surface/ water mass ($\text{m}^2.\text{kg}^{-1}$)	600	15	540	13.5	540	13.5
Rainy days per week	3	1	3	1	3	1

^aFor 1 m^2 parcel.

Table B1. Experimental Results for the First Set of Experiments

		Sample	pH	Eh (mV)
<i>Time = 12 Months</i>				
Anoxic Atmosphere	Flood Basalt	<i>fine</i>	6.6	8.9
		<i>coarse</i>	6.5	13
	Granodiorite	<i>fine</i>	6.3	5.9
		<i>coarse</i>	6.0	6.8
	Tonalite	<i>fine</i>	6.5	18
		<i>coarse</i>	6.6	14
Oxic Atmosphere	Flood Basalt	<i>fine</i>	7.2	12.2
		<i>coarse</i>	6.9	40.3
	Granodiorite	<i>fine</i>	7.2	62.2
		<i>coarse</i>	7.2	20.1
	Tonalite	<i>fine</i>	7.3	29.9
		<i>coarse</i>	7.1	50
<i>Time = 6 Months</i>				
Anoxic Atmosphere	Flood Basalt	<i>fine</i>	6.5	26.2
		<i>coarse</i>	6.3	16.4
	Granodiorite	<i>fine</i>	6.3	16.4
		<i>coarse</i>	6.3	34.4
	Tonalite	<i>fine</i>	6.3	52.4
		<i>coarse</i>	6.6	18.0
Oxic Atmosphere	Flood Basalt	<i>fine</i>	7.5	39.3
		<i>coarse</i>	7.5	40.9
	Granodiorite	<i>fine</i>	7.7	40.9
		<i>coarse</i>	7.4	26.2
	Tonalite	<i>fine</i>	8.8	16.4
		<i>coarse</i>	7.4	14.7
<i>Time = 3 Months</i>				
Anoxic Atmosphere	Flood Basalt	<i>fine</i>	6.2	66.7
		<i>coarse</i>	6.4	61.7
	Granodiorite	<i>fine</i>	5.6	64.3
		<i>coarse</i>	6.3	60.4
	Tonalite	<i>fine</i>	5.9	48.0
		<i>coarse</i>	6.2	65.8
Oxic Atmosphere	Flood Basalt	<i>fine</i>	5.9	91.2
		<i>coarse</i>	6.1	99.2
	Granodiorite	<i>fine</i>	6.1	59.0
		<i>coarse</i>	5.9	67.0
	Tonalite	<i>fine</i>	5.8	32.2
		<i>coarse</i>	5.9	96.5
<i>Monitor Time = 12 Months</i>				
Present Atmosphere	Flood Basalt	<i>fine</i>	7.6	389.2
		<i>coarse</i>	7.1	275.8
	Granodiorite	<i>fine</i>	7.9	239.2
		<i>coarse</i>	7.7	167.2
	Tonalite	<i>fine</i>	7.7	167.2
		<i>coarse</i>	7.7	245.2

Table B2. Experimental Results for the Second Set of Experiments

	Time	Sample	pH	Eh (mV)
Anoxic Atmosphere	5 days	<i>Flood Basalt</i>	5.63	50.7
		<i>Granodiorite</i>	4.99	98.3
		<i>Tonalite</i>	5.03	86.4
	15 days	<i>Flood Basalt</i>	5.93	55.3
		<i>Granodiorite</i>	5.4	87.0
		<i>Tonalite</i>	5.63	73.3
	30 days	<i>Flood Basalt</i>	5.95	54.7
		<i>Granodiorite</i>	5.47	83.5
		<i>Tonalite</i>	5.84	61.3
	45 days	<i>Flood Basalt</i>	6	51.7
		<i>Granodiorite</i>	5.67	71.1
		<i>Tonalite</i>	5.82	62.3
60 days	<i>Flood Basalt</i>	6.05	47.9	
	<i>Granodiorite</i>	5.63	72.4	
	<i>Tonalite</i>	5.81	60.1	
90 days	<i>Flood Basalt</i>	6.26	36.8	
	<i>Granodiorite</i>	5.87	59.4	
	<i>Tonalite</i>	6.03	50.3	
150 days	<i>Flood Basalt</i>	6.36	32.5	
	<i>Granodiorite</i>	6.27	37.9	
	<i>Tonalite</i>	6.29	36.7	
Present Atmosphere	150 days	<i>Flood Basalt</i>	7.2	324.6
		<i>Granodiorite</i>	7.25	379.4
		<i>Tonalite</i>	7.06	180.6

anoxic (duration 1 year long), whereas Table B2 refers to anoxic alone (duration 5 months).

Acknowledgments

[65] The authors would like to thank T. Aigouy, C. Boucayrand, C. Cavaré-Hester, E. Henry, S. Mounic, C. Causserand, F. and P. de Parseval for their technical assistance in the LMTG laboratory. A special thanks to S. Petit for performing FT-IR analysis at HydrASA Poitiers (France). We also thank the Editor L. Derry for his constructive comments. M. S. N. Carpenter post-edited the English style.

References

- Amrhein, C., and D. L. Suarez (1988), The use of a surface complexation model to describe the kinetics of ligand-promoted dissolution of anorthite, *Geochim. Cosmochim. Acta*, 52, 2785–2793, doi:10.1016/0016-7037(88)90146-9.
- Andrieux, P., and S. Petit (2010), Hydrothermal synthesis of dioctahedral smectites: The Al-Fe³⁺ chemical series: Part I: Influence of experimental conditions, *Appl. Clay Sci.*, 48(1–2), 5–17.
- Appelo, C. A. J., and D. L. Parkhurst (1999), User's guide to PHREEQC (version 2) - A computer program for speciation, batch-reaction, one-dimensional transport, and inverse calculations, *U.S. Geol. Surv. Water Resour. Invest. Rep.*, 99–4259.
- Berger, G., E. Cadore, J. Schott, and P. M. Dove (1994a), Dissolution rate of quartz in lead and sodium electrolyte solutions



- between 25° and 300°C: Effect of the nature of surface complexes and reaction affinity, *Geochim. Cosmochim. Acta*, **58**, 541–551, doi:10.1016/0016-7037(94)90487-1.
- Berger, G., C. Claparols, C. Guy, and V. Daux (1994b), Dissolution rate of a basalt glass in silica-rich solutions: Implications for long-term alteration, *Geochim. Cosmochim. Acta*, **58**, 4875–4886, doi:10.1016/0016-7037(94)90218-6.
- Berger, G., D. Beaufort, and J.-C. Lachapagne (2002), Experimental dissolution of sanidine under hydrothermal conditions: Mechanism and rate, *Am. J. Sci.*, **302**, 663–685, doi:10.2475/ajs.302.8.663.
- Berner, E. K., and R. A. Berner (1987), *The Global Water Cycle: Geochemistry of the Environment*, Prentice Hall, Englewoods Cliffs, N. J.
- Blum, A. E., and A. C. Lasaga (1991), The role of surface speciation in the dissolution of albite, *Geochim. Cosmochim. Acta*, **55**, 2193–2201, doi:10.1016/0016-7037(91)90096-N.
- Blum, A. E., and L. L. Stillings (1995), Feldspar dissolution kinetics, in *Chemical Weathering of Silicate Minerals*, *Rev. Mineral.*, vol. 31, edited by A. F. White and S. H. Brantley, pp. 565–581, Mineral. Soc. of Am., Washington D. C.
- Brady, P. V. (1991), The effect of silicate weathering on global temperature and atmospheric CO₂, *J. Geophys. Res.*, **96**, 18,101–18,106, doi:10.1029/91JB01898.
- Brantley, S. L. (2003), Reaction kinetics of primary rock-forming minerals under ambient conditions, in *Treatise on Geochemistry*, vol. 5, *Surface and Ground Water, Weathering, and Soils*, edited by J. I. Drever, pp. 73–117, Elsevier, Amsterdam, doi:10.1016/B0-08-043751-6/05075-1.
- Brantley, S. H., and Y. Chen (1995), Chemical weathering rates of pyroxenes and amphiboles, in *Chemical Weathering of Silicate Minerals*, *Rev. Mineral.*, vol. 31, edited by A. F. White and S. H. Brantley, pp. 119–168, Mineral. Soc. of Am., Washington D. C.
- Busenberg, E., and C. V. Clemency (1976), The dissolution kinetics of feldspars at 25°C and 1 atm CO₂ partial pressure, *Geochim. Cosmochim. Acta*, **40**, 41–49, doi:10.1016/0016-7037(76)90192-7.
- Chadwick, O., R. T. Gavenda, E. F. Kelly, K. Ziegler, C. G. Olson, W. Crawford Elliott, and D. M. Hendricks (2003), The impact of climate on biogeochemical functioning of volcanic soils, *Chem. Geol.*, **202**, 195–223, doi:10.1016/j.chemgeo.2002.09.001.
- Chou, L., and R. Wollast (1985), Steady state kinetics and dissolution mechanisms of albite, *Am. J. Sci.*, **285**, 963–993, doi:10.2475/ajs.285.10.963.
- Condie, K. C. (2001), Continental growth during formation of Rodinia at 1.35–0.9 Ga, *Gondwana Res.*, **4**, 5–16, doi:10.1016/S1342-937X(05)70650-X.
- Des Marais, D. J. (1994), The Archaean atmosphere: Its composition and fate, in *Archaean Crustal Evolution*, *Dev. Precambrian Geol.*, vol. 11, edited by K. C. Condie, pp. 505–519, Elsevier, Amsterdam.
- Dessert, C., B. Dupré, L. M. François, J. Schott, J. Gaillardet, G. Chakrapani, and S. Bajpaj (2001), Erosion of Deccan Traps determined by river geochemistry: Impact on the global climate and the ⁸⁷Sr/⁸⁶Sr ratio of seawater, *Earth Planet. Sci. Lett.*, **188**, 459–474, doi:10.1016/S0012-821X(01)00317-X.
- Dessert, C., B. Dupré, J. Gaillardet, L. M. François, and C. J. Allègre (2003), Basalt weathering laws and the impact of basalt weathering on the global carbon cycle, *Chem. Geol.*, **202**, 257–273.
- Dove, P. M., and D. A. Crerar (1990), Kinetics of quartz dissolution in electrolyte solutions using a hydrothermal mixed flow reactor, *Geochim. Cosmochim. Acta*, **54**, 955–969, doi:10.1016/0016-7037(90)90431-J.
- Eriksson, P. G., O. Catuneanu, D. R. Nelson, W. U. Mueller, and W. Altermann (Eds.) (2004), *The Precambrian Earth, Tempos and Events*, *Dev. Precambrian Geol.*, vol. 12, Elsevier, Amsterdam.
- Fetter, C. W. (1994), *Applied Hydrogeology*, 3rd ed., Prentice Hall, Upper Saddle River, N. J.
- Gaillardet, J., B. Dupré, P. Louvat, and C. J. Allègre (1999), Global silicate weathering and CO₂ consumption rates deduced from the chemistry of large rivers, *Chem. Geol.*, **159**, 3–30, doi:10.1016/S0009-2541(99)00031-5.
- Gautier, J. M., E. H. Oelkers, and J. Schott (1994), Experimental study of K-feldspar dissolution rates as a function of chemical affinity at 150°C and pH 9, *Geochim. Cosmochim. Acta*, **58**, 4549–4560, doi:10.1016/0016-7037(94)90190-2.
- Gislason, S. R., and S. Arnórsson (1993), Dissolution of primary basaltic minerals in natural waters: Saturation state and kinetics, *Chem. Geol.*, **105**, 117–135, doi:10.1016/0009-2541(93)90122-Y.
- Gislason, S. R., S. Arnórsson, and H. Armannsson (1996), Chemical weathering of basalt in southwest Iceland: Effects of runoff, age of rocks and vegetative/glacial cover, *Am. J. Sci.*, **296**, 837–907, doi:10.2475/ajs.296.8.837.
- Gladchenko, T. P., K. Hinz, O. Eldhom, H. Meyer, S. Neben, and J. Skojseid (1997), South Atlantic volcanic margin, *J. Geol. Soc.*, **154**, 465–470, doi:10.1144/gsjgs.154.3.0465.
- Gleizes, G., A. Nédélec, J.-L. Bouchez, and A. Autran (1993), Magnetic susceptibility of the Mont-Louis Andorra ilmenite-type granite (Pyrenees): A new tool for the petrographic characterization and regional mapping of zoned granite plutons, *J. Geophys. Res.*, **98**, 4317–4331, doi:10.1029/92JB01590.
- Hamilton, J. P., S. H. Brantley, C. G. Pantano, L. J. Criscenti, and J. D. Kubicki (2001), Dissolution of nepheline, jadeite and albite glasses: Toward better models for aluminosilicate dissolution, *Geochim. Cosmochim. Acta*, **65**, 3683–3702, doi:10.1016/S0016-7037(01)00724-4.
- Harry, D. L., and D. S. Sawyer (1992), Basaltic volcanism, mantle plumes, and the mechanism of rifting: the Parana flood basalt province of South America, *Geology*, **20**, 207–210.
- Hawkesworth, C. J., K. Gallagher, S. Kelley, M. Mantovani, D. W. Peate, M. Regelous, and N. W. Rogers (1992), Parana magmatism and the opening of the South Atlantic, in *Magmatism and the Causes of Continental Break-Up*, edited by B. C. Storey, T. Alabaster, and R. J. Pankhurst, *Geol. Soc. Spec. Publ.*, **68**, 221–240.
- Hawkesworth, C. J., K. Gallagher, L. Kirstein, M. S. Mantovani, M. D. Peate, and S. P. Turner (2000), Tectonic controls on magmatism associated with continental break-up: An example from the Paraná–Etendeka Province, *Earth Planet. Sci. Lett.*, **179**, 335–349, doi:10.1016/S0012-821X(00)00114-X.
- Hellmann, R. (1994), The albite-water system: Part I. The kinetics of dissolution as a function of pH at 100°, 200°, and 300°C, *Geochim. Cosmochim. Acta*, **58**, 595–611, doi:10.1016/0016-7037(94)90491-X.
- Higgins, J. A., and D. P. Schrag (2003), Aftermath of a snowball Earth, *Geophys. Geosyst.*, **4**(3), 1028, doi:10.1029/2002GC000403.
- Kasting, J. F. (1993), Earth's early atmosphere, *Science*, **259**, 920–926, doi:10.1126/science.11536547.
- Kasting, J. F., and J. L. Siefert (2002), Life and the evolution of Earth's atmosphere, *Science*, **296**, 1006–1068, doi:10.1126/science.1071184.



- Kerrick, D. M. (2001), Present and past nonanthropogenic CO₂ degassing from the solid Earth, *Rev. Geophys.*, *39*, 565–585, doi:10.1029/2001RG000105.
- Kirstein, L. A., S. Kelley, C. Hawkesworth, S. Turner, M. Mantovani, and J. Wijbrans (2001), Protracted felsic magmatic activity associated with the opening of the South Atlantic, *J. Geol. Soc.*, *158*, 583–592, doi:10.1144/jgs.158.4.583.
- Knauss, K. G., and S. A. Copenhaver (1995), The effect of malonate on the dissolution kinetics of albite, quartz and microcline as a function of pH and time at 70°C, *Appl. Geochem.*, *10*, 17–33, doi:10.1016/0883-2927(94)00045-8.
- Knauss, K. G., and T. J. Wolery (1986), Dependence of albite dissolution kinetics on pH and time at 25°C and 70°C, *Geochim. Cosmochim. Acta*, *50*, 2481–2497, doi:10.1016/0016-7037(86)90031-1.
- Le Hir, G., Y. Donnadieu, Y. Godd ris, R. T. Pierrehumbert, G. P. Halverson, M. Macouin, A. N d lec, and G. Ramstein (2009), The snowball Earth aftermath: Exploring the limits of continental weathering processes, *Earth Planet. Sci. Lett.*, *277*, 453–463, doi:10.1016/j.epsl.2008.11.010.
- Lowe, D. R., and M. M. Tice (2004), Geological evidence for Archaean atmospheric and climatic evolution: Fluctuating levels of CO₂, CH₄ and O₂ with an overriding tectonic control, *Geology*, *32*, 493–496, doi:10.1130/G20342.1.
- Mansour, C., G. Berger, M. F doroff, G. Lef vre, A. Pag s, E. M. Pagaveau, H. Catalette, and S. Zanna (2010), Influence of temperature and reducing conditions on the sorption of sulphate on magnetite, *J. Colloid Interface Sci.*, *352*, 476–482, doi:10.1016/j.jcis.2010.08.014.
- Martin, H. (1994), The Archaean grey gneisses and the genesis of the continental crust, *Archaean Crustal Evolution*, *Dev. Precambrian Geol.*, vol. 11, edited by K. C. Condie, pp. 205–259, Elsevier, Amsterdam, doi:10.1016/S0166-2635(08)70224-X.
- Martin, H., and J. F. Moyen (2002), Secular changes in tonalite-trondhjemite-granodiorite composition as markers of the progressive cooling Earth, *Geology*, *30*, 319–322, doi:10.1130/0091-7613(2002)030<0319:SCITTG>2.0.CO;2.
- Meunier, A., A. Mas, D. Beaufort, P. Patrier, and P. Dudoignon (2008), Clay minerals in basalts-Hawaiiite rocks from Mururoa atoll (French Polynesia). II. Petrography and geochemistry, *Clays Clay Miner.*, *56*, 730–750, doi:10.1346/CCMN.2008.0560612.
- Nagy, K. L. (1995), Dissolution and precipitation kinetics of sheet silicates, in *Chemical Weathering of Silicate Minerals*, edited by A. F. White and S. L. Brantley, pp. 173–225, Mineral. Soc. of Am., Washington D. C.
- N d lec, A., E. N. Nsifa, and H. Martin (1990), Major and trace geochemistry of the Archaean Ntem plutonic complex (south Cameroon): Petrogenesis and crustal evolution, *Precambrian Res.*, *47*, 35–50, doi:10.1016/0301-9268(90)90029-P.
- Nesbitt, W., and G. M. Young (1982), Early proterozoic climates and plate motions inferred from major elements: Chemistry of lutites, *Nature*, *299*, 715–717, doi:10.1038/299715a0.
- Oelkers, E. H., and S. R. Gislason (2001), The mechanism, rates and consequences of basaltic glass dissolution: I. An experimental study of the dissolution rates of a basaltic glass as a function of aqueous Al, Si and oxalic acid concentration at 25°C and pH=3 and 1, *Geochim. Cosmochim. Acta*, *65*, 3671–3681, doi:10.1016/S0016-7037(01)00664-0.
- Oelkers, E. H., J. Schott, and J. L. Devidal (1994), The effect of Al, pH and chemica affinity on the rates of aluminosilicates dissolution reactions, *Geochim. Cosmochim. Acta*, *58*, 2011–2024, doi:10.1016/0016-7037(94)90281-X.
- Oliva, P., J. Viers, and B. Dupr  (2003), Chemical weathering in granitic crystalline environments, *Chem. Geol.*, *202*, 225–256, doi:10.1016/j.chemgeo.2002.08.001.
- Pavlov, A. A., J. F. Kasting, J. L. Eigenbrode, and K. H. Freeman (2001), Organic haze in Earth’s early atmosphere: Source of low ¹³C late Archean kerogens?, *Geology*, *29*, 1003–1006, doi:10.1130/0091-7613(2001)029<1003:OHI-ESE>2.0.CO;2.
- Petit, S. (2006), Fourier Transform Infrared Spectroscopy, in *Handbook of Clay Science*, *Dev. Clay Sci.*, vol. 1, edited by F. Bergaya, B. K. G. Theng, and G. Lagaly, chap. 12.6, pp. 909–918, Elsevier, Oxford, U. K.
- Polv , M., R. C. Maury, H. Bellon, C. Rangin, B. Priadi, S. Yuwono, J. L. Joron, and R. Soeria Amata (1997), Magmatic evolution of Sulawesi (Indonesia): Constraints on the Cenozoic geodynamic history of the Sundaland active margin, *Tectonophysics*, *272*, 69–92, doi:10.1016/S0040-1951(96)00276-4.
- Renne, P. R., M. Ernesto, I. C. Pacca, R. S. Coe, J. M. Glen, M. Pr vot, and M. Perin (1992), The age of the Parana flood volcanism, rifting of Gondwanaland, and the Jurassic-Cretaceous boundary, *Science*, *258*, 975–979, doi:10.1126/science.258.5084.975.
- Renne, P. R., K. Deckart, M. Ernesto, G. F raud, and E. M. Piccirillo (1996), Age of the Ponta Grossa dike swarm (Brazil), and implications to Parana flood volcanism, *Earth Planet. Sci. Lett.*, *144*, 199–211, doi:10.1016/0012-821X(96)00155-0.
- Rose, N. M. (1991), Dissolution rates of prehnite, epidote, and albite, *Geochim. Cosmochim. Acta*, *55*, 3273–3286, doi:10.1016/0016-7037(91)90488-Q.
- Rye, R., P. H. Kuo, and H. D. Holland (1995), Atmospheric carbon dioxide concentrations 2.2 billions years ago, *Nature*, *378*, 603–605, doi:10.1038/378603a0.
- Schenato, F. (1997), Altera o pos-magmatica de um derrame basaltico (regiao de estancia velha), por ao sudeste da Bacia do Parana, RS, Brasil: Processos de resfriamento e vesicula o, Ph. D. thesis, Univ. Fed. do Rio Grande do Sul, Rio Grande do Sul, Brazil.
- Schott, J., and E. H. Oelkers (1993), The rate of dissolution and crystallization of silicates at hydrothermal conditions, paper presented at the Fourth International Symposium on Hydrothermal Reactions, Int. Assoc. of Geochem. and Cosmochemistry, Nancy, France.
- Schweda, P. (1989), Kinetics of alkali feldspar dissolution at low temperature, paper presented at the Sixth International Symposium on Water-Rock Interaction, Int. Assoc. of Geochem. and Cosmochemistry, Malvern, U. K.
- Scopel, R. M. (1997), Etude des coul es basaltiques   am thystes de la r gion de Ametista do Sul, RS-Br sil. Altera o post-magmatique, Rio Grande do Sul (Br sil), Ph. D. thesis, Univ. of Poitiers, Poitiers, France.
- Shang, C. K., M. Satir, W. Siebel, E. N. Nsifa, H. Taubald, J.-P. Li geois, and F. M. Tchoua (2004), TTG magmatism in the Congo craton: A view from major and trace element geochemistry, Rb-Sr and Sm-Nd systematics: Case of the Sangmelima region, Ntem complex, southern Cameroon, *J. Afr. Earth Sci.*, *40*, 61–79, doi:10.1016/j.jafrearsci.2004.07.005.
- Sigfusson, B., S. R. Gislason, and G. I. Paton (2006), The effect of soil solution chemistry on the weathering rate of a Histic Andosol, *J. Chem. Explor.*, *88*, 321–324.



- Strickland, J. D. H., and T. R. Parsons (1972), Determination of reactive silicate, in *A Practical Handbook of Seawater Analysis*, *Bull. Fish. Res. Board Can.*, 61, 65–70.
- Veldkamp, E., and A. G. Jongman (1990), Weathering of alkaline basalt gravel in two older alluvial river terraces, Limagne, France, *Chem. Geol.*, 84, 148–149, doi:10.1016/0009-2541(90)90193-B.
- Vingiani, S., F. Terribile, A. Meunier, and S. Petit (2010), Weathering of basaltic pebbles in a red soil from Sardinia: A microsite approach for the identification of secondary mineral phases, *Catena*, 83(2–3), 96–106.
- Walker, C. G. (1990), Precambrian evolution of the climate system, *Palaeogeogr. Palaeoclimatol. Palaeoecol.*, 82, 261–289.
- Walker, J. G. C., P. B. Hays, and J. F. Kasting (1981), A negative feedback mechanism for the long-term stabilization of Earth's surface temperature, *J. Geophys. Res.*, 86, 9776–9782, doi:10.1029/JC086iC10p09776.
- Wedepohl, K. H. (1995), The composition of the continental crust, *Geochim. Cosmochim. Acta*, 59, 1217–1232, doi:10.1016/0016-7037(95)00038-2.
- Whipkey, C. E., R. C. Capo, J. C. C. Hsieh, and O. Chadwick (2002), Development of magnesian carbonates in Quaternary soils on the Island of Hawaii, *J. Sediment. Res.*, 72, 158–165, doi:10.1306/050801720158.
- White, A. F. (1983), Surface chemistry and dissolution kinetics of glassy rocks at 25°C, *Geochim. Cosmochim. Acta*, 47, 805–815, doi:10.1016/0016-7037(83)90114-X.
- White, A. F., and A. E. Blum (1995), Effects of climate on chemical weathering in watersheds, *Geochim. Cosmochim. Acta*, 59, 1729–1747, doi:10.1016/0016-7037(95)00078-E.
- White, A. F., and S. L. Brantley (2003), The effect of time on the weathering of silicate minerals: why do weathering rates differ in the laboratory and field?, *Chem. Geol.*, 202, 479–506.
- White, A. F., and H. C. Claassen (1980), Kinetic model for the short-term dissolution of a rhyolitic glass, *Chem. Geol.*, 28, 91–109, doi:10.1016/0009-2541(80)90038-8.
- Wollast, R., and L. Chou (1992), Surface reactions during the early stages of weathering of albite, *Geochim. Cosmochim. Acta*, 56, 3113–3121, doi:10.1016/0016-7037(92)90292-Q.
- Young, G. M. (1991), The geological record of glaciation: Relevance to the climatic history of the Earth, *Geosci. Can.*, 18, 100–108.